Quasinormal modes and their excitation beyond general relativity

Hector O. Silva[,1] Giovanni Tambalo[,2,1] Kostas Glampedakis[,3,4] Kent Yagi[,5] and Jan Steinhoff[1]

[1]*Max Planck Institute for Gravitational Physics (Albert Einstein Institute), D-14476 Potsdam, Germany*
[2]*Institut für Theoretische Physik, ETH Zürich, 8093 Zürich, Switzerland*
[3]*Departamento de Física, Universidad de Murcia, Murcia, E-30100, Spain*
[4]*Theoretical Astrophysics, University of Tübingen, Auf der Morgenstelle 10, D-72076 Tübingen, Germany*
[5]*Department of Physics, University of Virginia, Charlottesville, Virginia 22904, USA*

The response of black holes to small perturbations is known to be partially described by a superposition of quasinormal modes. Despite their importance to enable strong-field tests of gravity, little to nothing is known about what overtones and quasinormal-mode amplitudes are like for black holes in extensions to general relativity. We take a first step in this direction and study what is arguably the simplest model that allows first-principle calculations to be made: a nonrotating black hole in an effective-field-theory extension of general relativity with cubic-in-curvature terms. Using a phase-amplitude scheme that uses analytical continuation and the Prüfer transformation, we numerically compute, for the first time, the quasinormal overtone frequencies (in this theory) and quasinormal-mode excitation factors (in any theory beyond general relativity). We find that the overtone quasinormal frequencies and their excitation factors are more sensitive than the fundamental mode to the length scale l introduced by the higher-derivative terms in the effective field theory. We argue that a description of all overtones cannot be made within the regime of validity of the effective field theory, and we conjecture that this is a general feature of any extension to general relativity that introduces a new length scale. We also find that a parametrization of the modifications to the general-relativistic quasinormal frequencies in terms of the ratio between l and the black hole's mass is somewhat inadequate, and we propose a better alternative. As an application, we perform a preliminary study of the implications of the breakdown, in the effective field theory, of the equivalence between the quasinormal mode spectra associated to metric perturbations of polar and axial parity of the Schwarzschild black hole in general relativity. We also present a simple justification for the loss of isospectrality.

I. INTRODUCTION

The study of the response of black holes to external perturbations has a long history that dates back to the seminal work of Regge and Wheeler on the stability of the "Schwarzschild singularity" against linear perturbations in the 1950s [1]. Numerical scattering experiments performed by Vishveshwara [2] showed that the response in time of the black hole to incident Gaussian wave packets exhibits, after an initial prompt response, a characteristic damped oscillation, i.e., a "ringdown." The ringdown was also observed in the gravitational-waves signals produced by test particles plunging radially into black holes by Davis *et al.* [3–5] and in stellar collapse by Cunningham, Price

and Moncrief [6,7]. The latter showed that the ringdown has oscillation frequency and damping time in conformity with the quasinormal frequencies of a Schwarzschild black hole calculated by Chandrasekhar and Detweiler [8]. Chandrasekhar and Detweiler also proved a remarkable result: the spectrum of quasinormal modes associated to metric perturbations of axial parity (described by Regge-Wheeler equation [1]) and polar parity (described by the Zerilli equation [9,10]) are the same despite the different forms of these equations. The two spectra are said to be isospectral.

It was not until the work of Leaver [11] in the 1980s, that the relation between the source of disturbance and resulting gravitational-wave signal was studied analytically as an initial-value problem using Green's functions; see also, e.g., Refs. [12–18]. It became understood that the ringdown dominates the black hole's response, except at very early (the "prompt response") and very late times (the "tail" [19]), and that it consists of a superposition of quasinormal modes. The amplitude with which each mode contributes to the ringdown is determined by its excitation coefficient,

which can be factorized into perturbation independent (termed the "quasinormal-mode excitation factor") and dependent parts. Together, quasinormal modes and their excitation coefficients can be used to construct the quasinormal-mode contribution to the Green's function which, in turn, can be used to evolve an initial data in time. This approach has been used to reproduce the ringdown in the aforementioned cases [11,14].

The quasinormal frequencies of the astrophysically relevant Kerr solution are uniquely determined by the black hole's mass and spin [20]. The identification of two or more quasinormal frequencies from gravitational waves produced, e.g., in the coalescence of binary black holes [21–24], would enable "direct evidence of black holes with the same certainty as, say, the 21 cm line identifies interstellar hydrogen," as suggested by Detweiler [25]. If black hole spectroscopy ever reveals a tension between general relativistic predictions and observations, it would be suggestive of new physics beyond general relativity [26,27].

With the advent of gravitational-wave astronomy [28–30], it becomes sensible to attempt to understand the quasinormal mode spectra (and respective excitation) in theories beyond general relativity. In general relativity, an *ab initio* description of the ringdown for the astrophysically relevant case of comparable mass binary-black hole coalescence remains an outstanding open problem. However, as exemplified in the foregoing discussion, progress is possible within black hole perturbation theory.

Here we take an initial step in this direction. We study the quasinormal mode spectrum and the excitation factors of a nonrotating black hole in an effective field theory (EFT) of general relativity [31]; see the requirements for the construction of the EFT therein. The motivations behind this choice are manifold. First, the EFT has only two degrees of freedom, and we avoid unnecessary technical complications introduced by couplings between the metric and extra fields, such as scalars. Second, the EFT admits an exact analytical nonrotating black hole solution to which perturbation theory can be applied [32–36]. Third, previous analysis, that focused only on the lowest damped quasinormal frequencies, showed that isospectrality of perturbations of the Schwarzschild solution [8] is broken due to the higher-dimension EFT terms [32–34]. For these reasons, the EFT of general relativity is ideal to address from first principles the following questions, representative of what may be asked in any extension to general relativity,

    (i) *What is the consequence of the breakdown of isospectrality in realistic sources of gravitational radiation?*

    (ii) *How sensitive are quasinormal overtone frequencies to corrections to general relativity?*

We give preliminary answers to these questions here.

This work is organized as follows. In Sec. II, we review the EFT of general relativity and the black hole solution we will study. In Sec. III, we present the equations that describe the linear perturbations of this black hole. We compare our formulation of the equations with previous literature, and present a simple explanation for the absence of isospectrality in the EFT. In Sec. IV, we review a phase-amplitude method, developed by one of us [37], that we use to compute the quasinormal frequencies (including overtones) and their respective excitation factors. In Sec. V, we present our numerical results and discuss their regime of validity. In Sec. VI, we summarize and discuss our main results. We use the mostly plus metric signature and use geometrical units $c = G = 1$. Parenthesis are used to indicate index symmetrization, as in $T_{(\mu\nu)} = (T_{\mu\nu} + T_{\nu\mu})/2$.

II. EFFECTIVE-FIELD-THEORY OF GENERAL RELATIVITY

A. Action and field equations

The general structure of the action is

$$S = \frac{1}{16\pi} \int d^4x \sqrt{-g} R + \frac{1}{16\pi} \sum_{n \geq 2} l^{2n-2} S^{(2n)}, \quad (1)$$

where l is a length scale assumed to be small compared to the length scale associated with a black hole of mass M, i.e., $M \gg l$, and $S^{(2n)}$ is the action of the nth order curvature term which has $2n$ derivatives of the metric. For this reason we will use the terminology "dimension-$2n$ operator." Notice that only even powers in l are allowed from dimensional analysis.

One can show that, upon field redefinitions and as long as the EFT construction is built around vacuum GR, that no dimension-four operators exist. The first nontrivial contribution occurs at dimension six and, at this order, there are only two operators [38]. The resulting action is

$$S = \frac{1}{16\pi} \int d^4x \sqrt{-g} [R + l^4 \mathcal{L}], \quad (2)$$

where

$$\mathcal{L} = \lambda_e R_{\mu\nu}{}^{\rho\sigma} R_{\rho\sigma}{}^{\delta\gamma} R_{\delta\gamma}{}^{\mu\nu} + \lambda_o R_{\mu\nu}{}^{\rho\sigma} R_{\rho\sigma}{}^{\delta\gamma} \tilde{R}_{\delta\gamma}{}^{\mu\nu}, \quad (3)$$

and $\tilde{R}_{\mu\nu\rho\sigma} = (1/2)\epsilon_{\mu\nu}{}^{\alpha\beta} R_{\alpha\beta\rho\sigma}$, where $\epsilon_{\mu\nu\rho\sigma}$ is the totally antisymmetric Levi-Civita tensor, $\lambda_{e,o}$ are dimensionless constants associated to the even- ("e") and odd-parity ("o") curvature terms, and ℓ is a length scale.

The field equations of the theory, obtained by varying the action (2) with respect to $g^{\mu\nu}$, are

$$\mathcal{E}_{\alpha\beta} = G_{\alpha\beta} + l^4 \mathcal{S}_{\alpha\beta} = 0, \quad (4)$$

where

$$\mathcal{S}_{\alpha\beta} = P_{(\alpha}{}^{\rho\sigma\gamma}R_{\beta)\rho\sigma\gamma} - \frac{1}{2}g_{\alpha\beta}\mathcal{L} + 2\nabla^{\sigma}\nabla^{\rho}P_{(\alpha|\sigma|\beta)\rho}, \quad (5a)$$

$$P_{\alpha\beta\mu\nu} = 3\lambda_{\mathrm{e}}R_{\alpha\beta}{}^{\rho\sigma}R_{\rho\sigma\mu\nu}$$
$$+ \frac{3}{2}\lambda_{\mathrm{o}}(R_{\alpha\beta}{}^{\rho\sigma}\tilde{R}_{\rho\sigma\mu\nu} + R_{\alpha\beta}{}^{\rho\sigma}\tilde{R}_{\mu\nu\rho\sigma}). \quad (5b)$$

We will only consider the even-parity operator hereafter, i.e., we set $\lambda_{\mathrm{o}} = 0$. For brevity, we will write $\lambda_{\mathrm{e}} = \lambda$, and assume λ to be positive. *A priori*, however, λ can have either sign; see, e.g., Refs. [39–41]. We will work to leading order in λ, that is, to $\mathcal{O}(l^4)$. Other aspects of the EFT in the context of gravitational-wave physics are discussed, e.g., in Refs. [42–47] and references therein.

B. Nonrotating black hole solution

A nonrotating spherically symmetric black-hole solution of the theory (2) was found in Refs. [33,34,38]. The line element is

$$ds^2 = -N^2 f dt^2 + f^{-1}dr^2 + r^2 d\theta^2 + r^2 \sin^2\theta d\varphi^2, \quad (6)$$

where the metric functions N and f are, respectively,

$$N = 1 - 108\varepsilon\frac{M^6}{r^6}, \quad (7a)$$

$$f = 1 - \frac{2M}{r} + 216\varepsilon\left(1 - \frac{49}{27}\frac{M}{r}\right)\frac{M^6}{r^6}, \quad (7b)$$

and we introduced the dimensionless parameter,

$$\varepsilon = \lambda l^4/M^4, \quad (8)$$

and M is the Arnowitt-Deser-Misner (ADM) mass of the black hole. The event horizon r_{h} is located at the largest positive root of f,

$$r_{\mathrm{h}} = 2M(1 - 5\varepsilon/16). \quad (9)$$

The black-hole solution reduces to that of Schwarzschild in the limit $\lambda \to 0$, i.e., $\varepsilon \to 0$. We note that r_{h} can vanish if $\varepsilon = 16/5$ which, however, is outside the validity of the EFT, $\varepsilon \ll 1$. For the sake of completeness, we derive Eq. (6) in Appendix A. Further, in Appendix B, we show that the spacetime is of Petrov-type D.

The spacetime as written in Eq. (6) demands some care when r is approximately $2M$. To see this, take the g_{rr} metric component,

$$f^{-1} = [1 - 2M/r + \varepsilon\delta f(r)]^{-1}, \quad (10)$$

where we defined

$$\delta f = 216\frac{M^6}{r^6}\left(1 - \frac{49}{27}\frac{M}{r}\right). \quad (11)$$

As $r \to 2M$, we see that the EFT correction starts dominating over the general-relativistic term. This means that the expansion in ε ceases to hold in this limit. The same happens for $g_{tt} = -N^2 f$.

To resolve this issue we perform a "resummation." The idea is to factor out a multiplicative term $1 - r_{\mathrm{h}}/r$, thereby recasting either $N^2 f$ or f in the schematic form:

$$z(r) = (1 - r_{\mathrm{h}}/r)[1 + \varepsilon\delta z(r)], \qquad z \text{ arbitrary.} \quad (12)$$

In this way, we guarantee that $\mathcal{O}(\varepsilon)$ terms are small for any value of $r \geq r_{\mathrm{h}}$. We leave the details of this calculation to Appendix C and quote our final result:

$$N^2 f = \left(1 - \frac{r_{\mathrm{h}}}{r}\right)\left[1 - \varepsilon\left(\frac{5M}{8r} + \frac{5M^2}{4r^2} + \frac{5M^3}{2r^3} + \frac{5M^4}{r^4}\right.\right.$$
$$\left.\left. + \frac{10M^5}{r^5} + \frac{20M^6}{r^6}\right)\right], \quad (13a)$$

$$f^{-1} = \left(1 - \frac{r_{\mathrm{h}}}{r}\right)^{-1}\left[1 + \varepsilon\left(\frac{5M}{8r} + \frac{5M^2}{4r^2} + \frac{5M^3}{2r^3} + \frac{5M^4}{r^4}\right.\right.$$
$$\left.\left. + \frac{10M^5}{r^5} - \frac{196M^6}{r^6}\right)\right]. \quad (13b)$$

Equations (13a) and (13b) are the expressions we will use for the g_{tt} and g_{rr} metric components, respectively. By construction, both equations have the expected behavior at the event horizon r_{h}. In addition, since to $\mathcal{O}(\varepsilon)$,

$$N^2 f = f \simeq 1 - 2M/r + \mathcal{O}(r^{-2}), \qquad r/M \gg 1, \quad (14)$$

we have retained the interpretation of M being the ADM black-hole mass and that the spacetime is asymptotically Minkowski.

III. BLACK HOLE PERTURBATIONS

The linear gravitational perturbations of the black-hole solution (6) were analyzed in Refs. [33,34], in the Regge-Wheeler-Zerilli formalism ("metric-perturbation approach") [1,9,10], and in Refs. [35,36] in the Newman-Penrose [48] and Geroch-Held-Penrose [49] formalisms ("curvature-perturbation approach"). See also Refs. [50,51] for related work in the latter approach.

In the metric-perturbation approach, the problem reduces to studying two equations in the frequency domain

$$\left[\frac{d^2}{dx^2} + \frac{\omega^2}{c_{\mathrm{s}}^2(r)} - V_{\ell}^{(\pm)}(r)\right]X_{\ell\omega}^{(\pm)}(r) = 0, \quad (15)$$
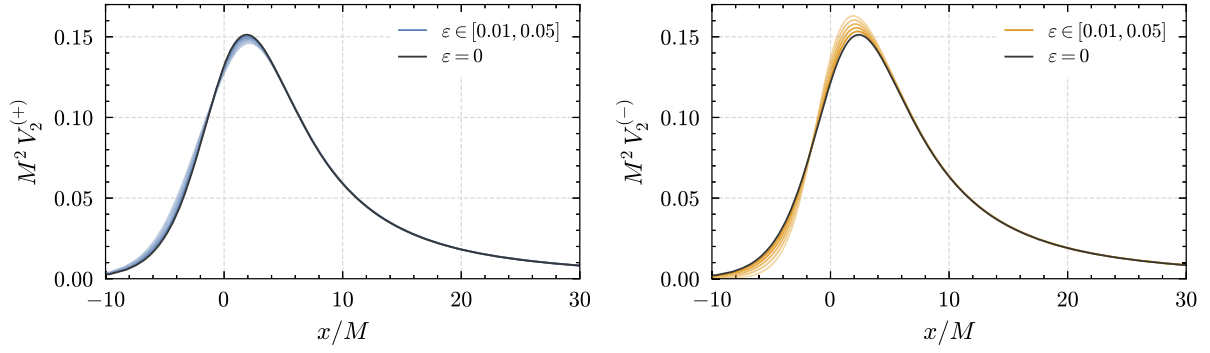
FIG. 1. The effective potentials $V_2^{(\pm)}$ for perturbations of polar (left panel) and axial (right panel) parity. We vary the parameter $\varepsilon = \lambda l^4/M^4$ from zero (general relativity) to 0.05 in increments of $\Delta\varepsilon = 0.01$. The value of the potential's peak decreases (increases) for the polar- (axial-) parity potentials with respect to general relativity. The location of the peak shifts in opposite directions, with respect to the case of general relativity: outwardly for polar-parity and inwardly for the axial-parity potential. These changes are bound to the region between the event horizon, pushed to $x \to -\infty$, and the location of the potential peak.

that we now describe in detail. The superscript $(\pm)$ is used to denote variables associated to metric perturbations of polar $(+)$ or axial $(-)$ parity, which we assume to have harmonic time-dependence $\exp(-i\omega t)$, and are labeled by the multipole index $\ell \geq 2$. Metric perturbations of polar and axial parities are fully described by a single master function known as the Zerilli $X^{(+)}$ and Regge-Wheeler $X^{(-)}$ functions, respectively.[1] We also introduced the tortoise coordinate x, defined as

$$dx/dr = 1/(Nf), \tag{16}$$

and that maps the domain $r_h \leq r < \infty$ to $-\infty < x < \infty$. This is not guaranteed to happen for all values of ε. As we detail in Appendix D, the desired mapping holds for $\varepsilon \lesssim 0.59$. Finally, $V_\ell^{(\pm)}$ and c_s^2 are the black-hole effective potential and propagation velocity of the perturbations, respectively. Let us consider both in turn.

First, the effective potential can be decomposed in a resummed form as

$$V_\ell^{(\pm)} = \left(1 - \frac{r_h}{r}\right)[\bar{V}_\ell^{(\pm)} + \varepsilon \delta V_\ell^{(\pm)}]. \tag{17}$$

The bare general-relativity contributions to the potential are the Zerilli [9] and Regge-Wheeler [1] potentials, given respectively by

$$\bar{V}_\ell^{(+)} = \frac{1}{(r\Lambda_\ell)^2}\left[2\lambda_\ell^2(\Lambda_\ell + 1) + \frac{18M^2}{r^2}\left(\lambda_\ell + \frac{M}{r}\right)\right], \tag{18a}$$

$$\bar{V}_\ell^{(-)} = \frac{1}{r^2}\left[\ell(\ell+1) - \frac{6M}{r}\right], \tag{18b}$$

where we defined

$$\lambda_\ell = (\ell+2)(\ell-1)/2, \quad \text{and} \quad \Lambda_\ell = \lambda_\ell + 3M/r. \tag{19}$$

The modifications to these potentials originating from the dimension-six operators can be written schematically as

$$\delta V_\ell^{(+)} = \frac{1}{(r\Lambda_\ell)^2}\sum_{i=1}^{10} v_{i\ell}^{(+)}(r)(M/r)^i, \tag{20a}$$

$$\delta V_\ell^{(-)} = \frac{1}{r^2}\sum_{i=1}^{7} v_{i\ell}^{(-)}(M/r)^i. \tag{20b}$$

The coefficients $v_{i\ell}^{(+)}$ contain Λ_ℓ for $n > 4$; hence the explicitly stated dependence on r. In contrast, $v_{i\ell}^{(-)}$ is independent of r for all n. All coefficients have powers of ℓ. We show the explicit forms of $v_{i\ell}^{(\pm)}$ in Appendix E.

In Fig. 1 we show both potentials, Eqs. (18a) and (18b), for $\ell = 2$ as functions of the tortoise coordinate x. The curves correspond to increasing values of ε, from zero (general relativity) to 0.05 in steps of $\Delta\varepsilon = 0.01$. The EFT corrections are most salient in the region between the event horizon and the location of the potential peak; past the latter the curves become identical to one another.

It is important to note that the potentials are short ranged, i.e., their integral on the domain $x \in (-\infty, +\infty)$ is finite. Indeed, one can verify that

$$\int_{-\infty}^{+\infty} V_\ell^{(\pm)} dx = \frac{1}{2M}\left[2\lambda_\ell + \frac{1}{2} + \varepsilon \iota_\ell^{(\pm)}\right], \tag{21}$$

where $\iota_\ell^{(+)} \neq \iota_\ell^{(-)}$ are parity-dependent functions of ℓ. In the limit of general relativity, the integrals of the Regge-Wheeler

---

[1]We verified that in the EFT, as in general relativity, the Zerilli [9] and Zerilli-Moncrief [52] functions and the Regge-Wheeler [1] and Cunningham-Price-Moncrief [6] functions satisfy the same homogeneous differential equations.

and Zerilli potentials are the same. This equality, first noticed by Chandrasekhar and Detweiler [8] (see also Refs. [53,54]), is a necessary condition to establish the isospectrality of the Regge-Wheeler and Zerilli potentials. More precisely, the equality of Eq. (21) is the first of an infinite hierarchy of integral equalities that must be satisfied by a pair of potentials if they are to have the same reflection and transmission coefficients.[2] That this equality is broken by the EFT corrections already at "zeroth order" in this hierarchy implies the breakdown of isospectrality.

Finally, perturbations of polar and axial parity propagate with a position-dependent velocity

$$
\begin{aligned}
c_{\mathrm{s}}^2 &= 1 - 288 \varepsilon f \frac{M^5}{r^5}, \\
&\simeq 1 - 288 \varepsilon \left(1 - \frac{r_{\mathrm{h}}}{r}\right) \frac{M^5}{r^5},
\end{aligned}
\tag{22}
$$

where in the second line we used the resummed form of f [cf. Eq. (13b)] and kept the $\mathcal{O}(\varepsilon)$ term only. We may note that c_{s}^2 is unity at spatial infinity and at the event horizon r_{h}, while it can be sub- or superluminal outside r_{h} depending on the sign of ε. Reference [58] argues that this speed cannot be used to predict time delay (or advance) with respect to general relativity as long as one stays within the regime of validity of the EFT.

Before proceeding, let us compare our Eq. (15) with those found in the literature, particularly in the works by de Rham *et al.* [33] and Cano *et al.* [34] who, like ourselves, worked in metric perturbation approach. In comparison to Ref. [33], our perturbation equations are similar to their Eqs. (2.23) except that we did a resummation of the effective potentials. Likewise, we use the same definition of the tortoise coordinate, though, again, we perform a resummation. To compute the quasinormal mode frequencies, Ref. [33] recasts their equations in a form that can be mapped into the quasinormal frequency parametrization of Ref. [59]. In comparison to Ref. [34], our perturbation equations are different both in the choice of the tortoise coordinate [they use a "pseudotortoise coordinate"; see Eq. (41) therein] and in the effective potentials (they do a field redefinition to trade the position-dependent propagation speed c_{s}^2 for a frequency-dependent potential). To compute the quasinormal frequencies, Ref. [34] did a direct integration of the perturbation equations.[3]

Cano *et al.* [34] reports an agreement of approximately 1% to 5% of their results with those of de Rham *et al.* [33]. In another work, Cano *et al.* [36] also computed the quasinormal frequencies for rotating black holes using the curvature-perturbation approach and using a small spin expansion [35]. They followed the approach of Ref. [50] to compute the quasinormal frequencies, and the results were cross-checked against the direct integration of the modified Teukolsky equation. In the nonrotating limit, their results agree with those of Refs. [33,34]. Our results will be presented in Sec. V. However, first, let us motivate and explain the phase-amplitude method we will adopt to compute the quasinormal modes and their excitation.

IV. QUASINORMAL MODES AND THEIR EXCITATION

In this section, we review the "quick and dirty" phase-amplitude method developed by Glampedakis and Andersson [37] for studying black-hole resonances. We will first review some technical difficulties in numerically computing quasinormal modes and how they are overcome in the phase-amplitude approach. We will then explain how the quasinormal-mode excitation factors can be determined.

A. Quasinormal modes

We are interested in computing the quasinormal modes associated to Eq. (15). Because the effective potentials are short ranged and vanish both at the horizon and at spatial infinity, whereat the propagation speed c_{s}^2 becomes unity, the general physical solution of Eq. (15) has the form

$$
X_{\ell\omega}^{(\pm)} \simeq \begin{cases} \mathrm{e}^{-\mathrm{i}\omega x} & x \to -\infty \\ A_{\ell\omega}^{(\pm),\mathrm{in}} \mathrm{e}^{-\mathrm{i}\omega x} + A_{\ell\omega}^{(\pm),\mathrm{out}} \mathrm{e}^{+\mathrm{i}\omega x} & x \to +\infty \end{cases}, \tag{23}
$$

consisting of purely ingoing waves at the event horizon and a mixture of ingoing and outgoing waves at spatial infinity. From the ratio between the amplitudes of the ingoing and outgoing waves at spatial infinity, we can define the scattering matrix

$$
\mathcal{S}_{\ell\omega}^{(\pm)} = (-1)^{\ell+1} A_{\ell\omega}^{(\pm),\mathrm{out}} / A_{\ell\omega}^{(\pm),\mathrm{in}} = \exp[2\mathrm{i}\delta_{\ell\omega}^{(\pm)}], \tag{24}
$$

where $\delta_{\ell\omega}^{(\pm)}$ is the phase-shift function. Quasinormal modes are solutions defined by having $A_{\ell\omega}^{(\pm),\mathrm{in}} = 0$, i.e., they are the poles of the scattering matrix [2]. The problem of computing the quasinormal-mode frequencies $\omega_{\ell n}$ hence reduces to a boundary-value problem in which one has to find $\omega_{\ell n}$ such that $A_{\ell\omega}^{(\pm),\mathrm{in}}$ vanishes. Root-finding algorithms can be used to perform this task. In black-hole physics, for each multipole ℓ, there is an infinite number n of quasinormal frequencies that we sort according to their damping time. The index $n = 0$ is used for quasinormal-mode frequency

---

[2]These integrals are formally related to conserved quantities allowed by the Korteweg-de Vries equation [55]. See Ref. [53], Sec. 4 and its Appendix, for a discussion, and Refs. [56,57] for recent literature.

[3]Implicitly, Ref. [33] also does a direct integration of the perturbations equations. The reason is that the theory-agnostic coefficients in Ref. [59] are found by direct integration of their parametrized perturbation equation; see Eq. (10) and Sec. III therein.

with longest decay time (the "fundamental mode") and modes with $n > 0$ are called "overtones."

A numerical challenge immediately presents itself if one attempts to carry such procedure by numerically integrating the differential equation (15). Since $\omega_{\ell n}$ is complex-valued, we find

$$X_{\ell\omega}^{(\pm)} \simeq \exp(\mp x\,\mathrm{Im}\,\omega_{\ell n}), \qquad x \to \pm\infty. \tag{25}$$

and because $\mathrm{Im}\,\omega_{\ell n}$ is negative for stable perturbations, the quasinormal-mode solution diverges as $x \to \pm\infty$. Consequently, in the root-finding process, we must resolve an exponentially decaying from an exponentially growing part of the solution, at large values of x. This is even more challenging for overtones which, by definition, have shorter damping times.

B. The phase-amplitude method

Reference [37] proposed a "quick-and-dirty" method for the calculation of the quasinormal-mode frequencies that combines two ideas. First, instead of working with the (possibly rapidly varying) function $X_{\ell\omega}^{(\pm)}$, one works with slowly varying phase functions. Second, instead of working on the real axis, one performs an analytical continuation of $X_{\ell\omega}^{(\pm)}$ to complex values of x and a suitable integration path is chosen in order to balance the exponentially decaying and growing waves of the general solution Eq. (15). Let us see how this works in practice. To lighten the notation, we will omit the parity "$(\pm)$" and mode "$\ell\omega$" scripts for now.

We start by rewriting Eq. (15) as

$$\left[\frac{\mathrm{d}^2}{\mathrm{d}x^2} + Q\right] X = 0, \qquad Q = \omega^2/c_{\mathrm{s}}^2 - V, \tag{26}$$

where $Q \to \omega^2$ as $x \to \pm\infty$, and the boundary conditions (23) as follows:

$$X \simeq \begin{cases} e^{-\mathrm{i}\omega x} & x \to -\infty \\ B\sin(\omega x + \zeta) & x \to +\infty \end{cases}, \tag{27}$$

where B and ζ are complex-valued constants. Equation (26) admits an exact solution in the form

$$X = \exp\left[\int P(x')\mathrm{d}x'\right], \tag{28}$$

where P is the *phase function*,

$$P = \mathrm{d}\log X/\mathrm{d}x, \tag{29}$$

which, from Eq. (26), satisfies the Riccati equation[4]

$$\mathrm{d}P/\mathrm{d}x + P^2 + Q = 0, \tag{30}$$

and the quasinormal-mode boundary conditions translate into $P \to -\mathrm{i}\omega$ as $x \to -\infty$.

Instead of working with P as $x \to \infty$ as well, it is useful to introduce a second phase function, $\tilde{P}$, by means of the *Prüfer transformation* defined as:

$$X = B\sin[\omega x + \tilde{P}(x)], \tag{31a}$$

$$\mathrm{d}X/\mathrm{d}x = B\omega\cos[\omega x + \tilde{P}(x)]. \tag{31b}$$

We can calculate $\mathrm{d}\log X/\mathrm{d}x$ with the foregoing equations and find that the phase functions P and $\tilde{P}$ are related by

$$P = \omega\cot(\omega x + \tilde{P}), \tag{32}$$

with inverse

$$\tilde{P} = -\omega x + \frac{1}{2\mathrm{i}}\log\left[\frac{\mathrm{i}P - \omega}{\mathrm{i}P + \omega}\right]. \tag{33}$$

Note that Eq. (32) explains the absence of a $\mathrm{d}\tilde{P}/\mathrm{d}x$ term in Eq. (31b). A short calculation shows that the Prüfer phase function satisfies

$$\mathrm{d}\tilde{P}/\mathrm{d}x + (\omega - Q/\omega)\sin^2(\omega x + \tilde{P}) = 0. \tag{34}$$

From the asymptotic properties of Q and P, we find from Eqs. (30) and (34) that for real ω and ℓ,

$$\mathrm{d}P/\mathrm{d}x \simeq 0, \qquad x \to -\infty \tag{35a}$$

$$\mathrm{d}\tilde{P}/\mathrm{d}x \simeq 0, \qquad x \to +\infty \tag{35b}$$

That is, P and $\tilde{P}$ are slowly varying functions as $x \to -\infty$ and $x \to \infty$, respectively.[5] It is then suggestive that we should work with P in the domain $x \in (-\infty, x_{\mathrm{m}}]$ and with $\tilde{P}$ in the domain $x \in (x_{\mathrm{m}}, \infty)$, where x_{m} is a matching point. Experience has shown that the computation of the quasinormal frequencies does not depend on the precise value of x_{m}, as long as we chose it to be near the peak of the effective potential V [37]. Here we chose $r_{\mathrm{m}} = 3M$, the location of the light ring in the Schwarzschild spacetime, which translates to $x_{\mathrm{m}} \simeq 1.61M$.

Finally, we can compare Eqs. (31a) and (27) to conclude that $\tilde{P} \to \zeta$ as $x \to \infty$ and, by comparing Eqs. (23) and (27), that

---

[4]We may, parenthetically here, remark that the advantage of working with the Riccati equation had already been appreciated by Chandrasekhar and Detweiler [8]; cf. pp. 451 therein.

[5]Equations (30) and (34) can be used to compute Regge poles [37]. Like quasinormal modes, they are poles of the scattering matrix (24), but correspond instead to complex values of ℓ for a given real-valued ω. Regge poles are important in scattering theory; see, e.g., Refs. [60–62] for applications in black-hole physics.
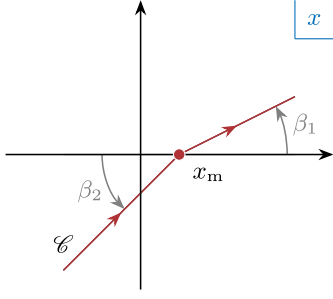
FIG. 2. The integration path $\mathcal{C}$ in the complex x-plane used for the calculation of the quasinormal modes. The value of $\beta_{1,2}$ is the chosen based on the asymptotic behavior of Q as $x \to \pm\infty$. In our problem, $\beta_{1,2} = -\arg\omega$. However, the method can be applied to other situations where this is not the case, such as of perturbations of the Kerr black hole [37].

$$A_{in}/A_{out} = -\exp(-2i\zeta). \tag{36}$$

The second step in the scheme of Ref. [37] consists in promoting the tortoise coordinate x to become complex valued as in, e.g., in the closely related phase-integral approach [63]. Consider the curve $\mathcal{C}$ illustrated in Fig. 2,

$$x = x_m + \rho\exp(i\beta), \tag{37}$$

parametrized by the real parameter $\rho \in (-\infty, \infty)$ and where β is a real constant. Note that the matching point is at $\rho = 0$. In terms of Eq. (37), the Prüfer equation (34) becomes

$$d\tilde{P}/dx + (\omega - Q/\omega)\sin^2[\omega x_m + \omega\rho\exp(i\beta) + \tilde{P}] = 0. \tag{38}$$

The crucial step is to now observe that, with a suitable choice of β, we can make the ingoing and outgoing waves as $x \to \infty$ to be of comparable asymptotic amplitudes. This is achieved by choosing,

$$\beta = -\arg\omega, \tag{39}$$

such that the integration path is parallel to the anti-Stokes lines when $x \to \pm\infty$ [37]. Equation (38) becomes

$$d\tilde{P}/dx + (\omega - Q/\omega)\sin^2(\omega x_m + |\omega|\rho + \tilde{P}) = 0. \tag{40}$$

Note that now the argument term proportional to ρ is real and hence we eliminated the asymptotic exponential behavior of the amplitude.

We can then rewrite the differential equations (30) and (40) for the phase functions with ρ as an independent variable, and trade x in favor of r by means of Eq. (37). We obtain

$$\frac{dP}{d\rho} + e^{i\beta}(P^2 + Q) = 0, \tag{41a}$$

$$\frac{d\tilde{P}}{d\rho} + e^{i\beta}\left(\omega - \frac{Q}{\omega}\right)\sin^2(\omega x_m + |\omega|\rho + \tilde{P}) = 0, \tag{41b}$$

$$\frac{dr}{d\rho} - e^{i\beta}\frac{dr}{dx} = 0, \tag{41c}$$

where dr/dx and β are given by Eqs. (16) and (39), respectively.

Equation (41) constitutes the system of differential equations we need to integrate to compute the quasinormal frequencies. The integration procedure can be summarized as follows:

(1) Choose the values of ε, ℓ, and ω, and with the latter compute $\beta = -\arg\omega$.

(2) Determine the initial condition for r as $\rho \to -\infty$. We found it useful, particularly in the context of the integrations in the next section, to integrate Eq. (41c) from $\rho_m = 0$ (at which $r = 3M$) backward to, say, $\rho_{min} = -50M$. This fixes $r_{min} = r(\rho_{min})$.

(3) Set the initial condition for P at ρ_{min} using the leading-order Wentzel-Kramers-Brillouin (WKB) formula, that is, $P_{min} = -iQ(r_{min})^{1/2}$.

(4) Integrate Eqs. (41a) and (41c) from ρ_{min} to ρ_m, using r_{min} and P_{min} as initial conditions.

(5) Calculate $\tilde{P}(\rho_m)$ from $P(\rho_m)$, the result of the previous step, using Eq. (33).

(6) Switch to Prüfer phase function, that is, integrate Eqs. (41b) and (41c) from $\rho = \rho_m$ up to $\rho = \rho_{max}$. In practice, we often used $\rho_{max} \approx 10^4 M$. This gives us $\zeta \simeq \tilde{P}(\rho_{max})$.

(7) Calculate A_{in}/A_{out} using Eq. (36).

(8) Repeat steps 1 to 7, updating the value of ω until the quasinormal-mode boundary condition $A_{in} = 0$ is satisfied. This is a root-finding problem that we solve using Muller's method [64].

We implemented the foregoing steps in C++. The integration of the differential equations was performed with the Runge-Kutta-Fehlberg (7, 8) method, as implemented in Odeint [65], part of the Boost library [66]. Our implementation of Muller's method follows the pseudo-code found in the "Numerical Recipes," Chapter 9.2 [67]. We will present the numerical results of our quick-and-dirty quasinormal mode frequency computations in Sec. V A.

C. The excitation factors

Having explained how we compute the quasinormal-mode frequencies, we now present how we obtain their *excitation factors*. The excitation factors are complex-valued constants that are characteristic of a black-hole spacetime and partially determine the amplitude with which different quasinormal modes are excited given an initial source of disturbance [11,14].

In this context, we are interested in the inhomogeneous version of Eq. (26)

$$\left[\frac{d^2}{dx^2} + Q\right]X = s. \tag{42}$$

The source s can represent, in the Fourier domain, either the initial data of the function X in a spacelike hypersurface $t =$ constant, or an external source driving the perturbations X, for instance, a particle plunging into the black hole [10]. The Cauchy problem associated to Eq. (42) can be studied using Green's functions [68]. Leaver [11], showed that the contribution from the quasinormal modes to the response in time of X is given by

$$X(t, r) = -\mathrm{Re}\sum_n [C_n e^{-i\omega_n(t-x)}], \tag{43}$$

where the sum is over all quasinormal frequencies ω_n and C_n are the respective quasinormal excitation coefficients. The latter can be factorized as

$$C_n = B_n I_n, \tag{44}$$

where I_n is an integral over the source s and the solution of the homogeneous equation (15) at the quasinormal frequency ω_n,

$$I_n = \int_{-\infty}^{\infty} \mathrm{d}x' \, s(x') X_n(x')/A_{\mathrm{out}}, \tag{45}$$

and B_n are the source-independent excitation factors

$$B_n = \frac{A_{\mathrm{out}}}{2\omega_n} \left[\frac{\mathrm{d}A_{\mathrm{in}}}{\mathrm{d}\omega}\right]^{-1}_{\omega=\omega_n} = \frac{1}{2\omega_n} \frac{A_{\mathrm{out}}}{\alpha_n}, \tag{46}$$

where we approximated $A_{\mathrm{in}} \simeq \alpha_n(\omega - \omega_n)$ in the vicinity of the quasinormal-mode frequency ω_n. Hence, the excitation factors are related to the ingoing- and outgoing-wave amplitudes at spatial infinity at frequencies near ω_n.

Equation (46) is our main quantity of interest. To calculate it, we follow Ref. [37] again, which proposed a phase-amplitude based scheme to compute B_n; see also Ref. [14]. This means we must derive a relation between the wave-amplitudes in Eq. (46) and the phase-functions P and $\tilde{P}$. We begin by recalling that the general physical solution of Eq. (26) is an ingoing wave at the event horizon and a mixture of ingoing and outgoing waves at spatial infinity. If we were to integrate this solution first from a near-horizon location $x_{-\infty}$ up to a matching point x_{m} and from a far-field location x_{∞} down to the same x_{m}, we would express the result of these two integrations as

$$X_{\mathrm{L}}(x_{\mathrm{m}}) = \exp(\varphi_{\mathrm{L},-}), \tag{47a}$$

$$X_{\mathrm{R}}(x_{\mathrm{m}}) = \mathcal{A}\exp(\varphi_{\mathrm{R},+}) + \mathcal{B}\exp(\varphi_{\mathrm{R},-}), \tag{47b}$$

where $\mathcal{A}$ and $\mathcal{B}$ are complex amplitudes and the various φ are integrals over the phases, more precisely,

$$\varphi_{\mathrm{L},-} = \int_{x_{-\infty}}^{x_{\mathrm{m}}} P_{\mathrm{L},-}\mathrm{d}x', \qquad \varphi_{\mathrm{R},\pm} = \int_{x_{\infty}}^{x_{\mathrm{m}}} P_{\mathrm{R},\pm}\mathrm{d}x'. \tag{48}$$

In these expressions, we introduced the subscripts L (R) to indicate a function to the left (right) of the matching point x_{m}, and $+$ ($-$) to indicate the ingoing (outgoing) wave phase. The condition for Eq. (47) to be a solution of Eq. (26) is that the logarithmic derivatives of X_{L} and X_{R} are continuous at x_{m}:

$$P_{\mathrm{L},-} = \frac{P_{\mathrm{R},+} + (\mathcal{B}/\mathcal{A})P_{\mathrm{R},-}\exp(\varphi_{\mathrm{R},-} - \varphi_{\mathrm{R},+})}{1 + (\mathcal{B}/\mathcal{A})\exp(\varphi_{\mathrm{R},-} - \varphi_{\mathrm{R},+})}, \tag{49}$$

which we solve for $\mathcal{B}/\mathcal{A}$,

$$\frac{\mathcal{B}}{\mathcal{A}} = \frac{P_{\mathrm{R},+} - P_{\mathrm{L},-}}{P_{\mathrm{L},-} - P_{\mathrm{R},-}}\exp(\varphi_{\mathrm{R},-} - \varphi_{\mathrm{R},+}). \tag{50}$$

This is the first step of the derivation. The next step consists of finding a relation between $\mathcal{A}$ and $\mathcal{B}$ with the amplitudes A_{in} and A_{out}; cf. Eq. (23). By doing so, as detailed in Ref. [37], we can rewrite Eq. (50) as

$$\frac{A_{\mathrm{in}}}{A_{\mathrm{out}}} = \frac{P_{\mathrm{R},+} - P_{\mathrm{L},-}}{P_{\mathrm{L},-} - P_{\mathrm{R},-}}e^{\Phi}, \tag{51}$$

where we defined

$$\Phi = 2i\omega x_{\infty} + \varphi_{\mathrm{R},+} - \varphi_{\mathrm{R},-} - 2i\int_{x_{\infty}}^{\infty} \frac{Q - \omega^2}{Q^{1/2} + \omega}\mathrm{d}x'. \tag{52}$$

The final step is to take a derivative of Eq. (51) with respect to the frequency ω and evaluate the result at the quasinormal mode frequency ω_n using that (i) $P_{\mathrm{R},+}$ is equal to $P_{\mathrm{L},-}$ at $\omega = \omega_n$ (this is nothing but the "resonant condition" for the quasinormal mode [8]) and (ii) the linear approximation $A_{\mathrm{in}} \simeq \alpha_n(\omega - \omega_n)$. By doing so, we obtain

$$\frac{\alpha_n}{A_{\mathrm{out}}} = \frac{\Omega_{\mathrm{R},+} - \Omega_{\mathrm{L},-}}{P_{\mathrm{L},-} - P_{\mathrm{R},-}}e^{\Phi_n}, \qquad \Omega_{\mathrm{R/L},\pm} = \frac{\mathrm{d}P_{\mathrm{R/L},\pm}}{\mathrm{d}\omega}, \tag{53}$$

which is our final result [37]. We reiterate that all quantities in Eq. (53) are evaluated at $x = x_{\mathrm{m}}$ [i.e., $\rho = \rho_{\mathrm{m}}$; see Eq. (37)] and $\omega = \omega_n$. Once we have determined the value of $\alpha_n/A_{\mathrm{out}}$, we use Eq. (46) to calculate the excitation factor B_n of the quasinormal mode frequency ω_n.

How do we calculate the various terms entering Eqs. (53) and (52)? From these equations we identify two terms that are independent on the phase functions, namely

$$2i\omega_n x_{\infty}, \quad \text{and} \quad \mathcal{I} = -2i\int_{x_{\infty}}^{\infty} \frac{Q - \omega_n^2}{Q^{1/2} + \omega_n}\mathrm{d}x'. \tag{54}$$

The former is a constant, while the latter can be integrated analytically by first expanding the integrand in powers of

$1/x \approx 1/r$ (since $|x/r_{\rm h}| \gg 1$) and then integrating term by term. The integral is convergent in our case, for which $Q \simeq \omega^2$ and $dQ/dx \simeq 0$ as $x \to \infty$. We find:

$$\mathcal{I} = -\frac{i}{2\omega}\left[u_\infty \frac{d^2 Q}{du^2}\bigg|_{u=0} + \frac{u_\infty^2}{6}\frac{d^3 Q}{du^3}\bigg|_{u=0} + \dots \right], \quad (55)$$

where $u = 1/x$.

For the remaining terms, it is convenient to separate our discussion into quantities that are determined between $x \in [x_{-\infty}, x_{\rm m}]$ and $x \in (x_{\rm m}, x_\infty]$. Because we must evaluate the phase functions at a quasinormal frequency, it is useful to use the analytical continuation and the Prüfer transformation introduced in Sec. IV B. By doing so, we can write down two systems of first-order differential equations. Specifically, for $x \in [x_{-\infty}, x_{\rm m}]$, we need to integrate three equations

$$\frac{dP_{\rm L,-}}{d\rho} + e^{i\beta}(P_{\rm L,-}^2 + Q) = 0, \quad (56a)$$

$$\frac{d\Omega_{\rm L,-}}{d\rho} + e^{i\beta}\left[2P_{\rm L,-}\Omega_{\rm L,-} + \frac{dQ}{d\omega}\right] = 0, \quad (56b)$$

$$\frac{dr}{d\rho} - e^{i\beta}\frac{dr}{dx} = 0, \quad (56c)$$

with initial conditions at $\rho = \rho_{\rm min}$ given by

$$P_{\rm L,-} = iQ^{1/2}, \quad \text{and} \quad \Omega_{\rm L,-} = -\frac{1}{2P_{\rm L,-}}\frac{dQ}{d\omega}. \quad (57)$$

For $x \in (x_{\rm m}, x_\infty]$, we need to integrate six equations

$$\frac{d\tilde{P}_{\rm R,\pm}}{d\rho} + e^{i\beta}\left(\omega - \frac{Q}{\omega}\right)\sin^2(\tilde{P}_{\rm R,\pm} + |\omega|\rho + \omega x_{\rm m}) = 0, \quad (58a)$$

$$\frac{d\varphi_{\rm R,\pm}}{d\rho} - e^{i\beta}\omega\cot(\omega x + \tilde{P}_{\rm R,\pm}) = 0, \quad (58b)$$

$$\frac{d\Omega_{\rm R,+}}{d\rho} + e^{i\beta}\left[2\Omega_{\rm R,+}\omega\cot(\omega x + \tilde{P}_{\rm R,+}) + \frac{dQ}{d\omega}\right] = 0, \quad (58c)$$

$$\frac{dr}{d\rho} - e^{i\beta}\frac{dr}{dx} = 0. \quad (58d)$$

The initial conditions for $\varphi_{\rm R,\pm}$ and $\Omega_{\rm R,+}$ at $\rho = \rho_{\rm max}$ are

$$\varphi_{\rm R,\pm} = 0, \quad \text{and} \quad \Omega_{\rm R,+} = -\frac{1}{2P_{\rm R,+}}\frac{dQ}{d\omega}, \quad (59)$$

and to determine the initial condition for $\tilde{P}_{\rm R,\pm}$, we first use the WKB formula $P_{\rm R,\pm} = \pm iQ^{1/2}$ and then substitute the result in Eq. (33). In our case $dQ/d\omega = 2\omega c_{\rm s}^{-2}$.

Equations (56) and (58) constitute the two systems of differential equations we need to integrate to compute the quasinormal-mode excitation factors. The integration procedure can be summarized as follows:

(1) Choose the values of ε, ℓ, and *quasinormal mode frequency* ω_n, and with the latter compute $\beta = -\arg\omega_n$.

(2) Determine the initial conditions for r as $\rho \to \pm\infty$. We integrate Eq. (41c) from $\rho_{\rm m} = 0$ backward (forward) to, say, $\rho_{\rm min} = -40M$ ($\rho_{\rm max} = 2\times 10^4 M$). This fixes $r_{\rm min} = r(\rho_{\rm min})$ and $r_{\rm max} = r(\rho_{\rm max})$.

(3) Determine the other initial conditions for the dependent variables in the two integration domains, that is, at $\rho_{\rm min}$ and $\rho_{\rm max}$.

(4) Integrate the system of equations (56) and (58) from $\rho_{\rm min}$ to $\rho_{\rm m}$ and from $\rho_{\rm max}$ to $\rho_{\rm m}$, respectively.

(5) Calculate $P_{\rm R,\pm}(\rho_{\rm m})$ from $\tilde{P}_{\rm R,\pm}(\rho_{\rm m})$ using Eq. (32).

(6) Compute $\alpha_n/A_{\rm out}$ using Eqs. (52) and (53), and, finally, the excitation factor B_n using Eq. (46).

We implemented the foregoing steps in C++, adopting the same integration library as in our calculation of the quasinormal mode frequencies. We will present our results for the quasinormal-mode excitation factors in Sec. V B.

V. NUMERICAL RESULTS

A. The quasinormal mode spectrum

1. Comparison with the literature

Our calculation of the quasinormal-mode frequencies was validated in two ways. First, in the limit of general relativity, we compared our results against the well-known values for a Schwarzschild black hole, finding excellent agreement. Computation wise, we found that it was necessary to shift the matching point closer to the event horizon to accurately calculate the overtone frequencies. Above a certain overtone number, typically $n \gtrsim 4$, it becomes increasingly challenging to locate the quasinormal mode in the root-finding process. The reason is that the simple integration path (37) fails to approximate the more complex integration path necessary for determining high overtone quasinormal frequencies; see Refs. [63,69]. For this reason, we quote results up to $n = 3$.

As an example, for the fundamental and third overtone quadrupole quasinormal frequencies we obtain

$$M\omega_{20}^{(+)} = 0.37367169 - 0.088962318i, \quad (60a)$$

$$M\omega_{20}^{(-)} = 0.37367169 - 0.088962321i, \quad (60b)$$

and

$$M\omega_{23}^{(+)} = 0.25150495 - 0.70514814i, \quad (61a)$$

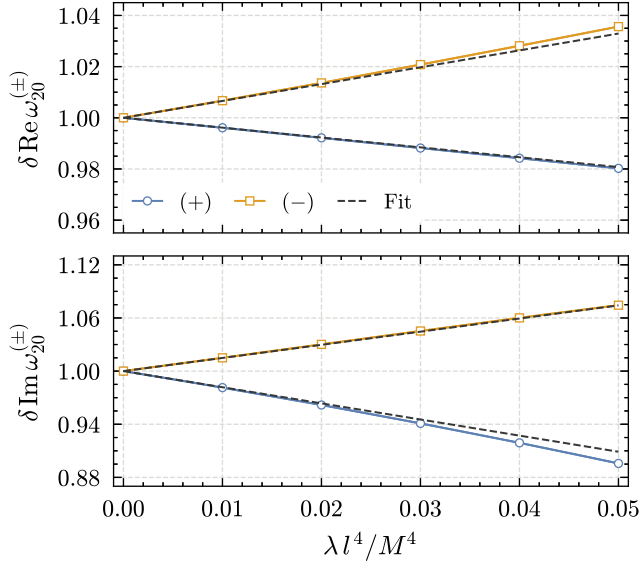$$M\omega_{23}^{(-)} = 0.25150496 - 0.70514818i, \quad (61b)$$

FIG. 3. The fundamental polar and axial quasinormal mode frequencies, normalized with respect to their Schwarzschild values, as functions of $\varepsilon = \lambda l^4/M^4$. The top panel shows the real part of frequencies, while the bottom panel their imaginary part. The markers distinguish curves corresponding to modes of polar $(+)$ and axial $(-)$ parities. The dashed lines are the linear fits by Cano *et al.* [36]. Both calculations agree remarkably well despite using two different forms of the perturbations equations to which different numerical techniques were applied to compute the quasinormal mode frequencies.

respectively. By isospectrality, we expect $\omega_{\ell n}^{(+)} = \omega_{\ell n}^{(-)}$, and, indeed, the phase-amplitude method yields quasinormal frequencies that differ from one another by $\mathcal{O}(10^{-6})$ or better. In addition, we compared our results against those of the QNM package [70] that uses the continued-fraction method of Refs. [20,71], and gives:

$$M\omega_{20}^{(\pm)} = 0.37367168 - 0.088962316i, \quad (62a)$$

$$M\omega_{23}^{(\pm)} = 0.25150496 - 0.70514820i. \quad (62b)$$

We find relative errors of $\mathcal{O}(10^{-6})$ that are largest for the highest overtone, $n = 3$, for the reason explained earlier. After having computed the general-relativistic quasinormal frequencies to good accuracy, we varied the EFT parameter ε in constant steps of $\Delta\varepsilon = 0.001$ and scanned the domain $\varepsilon \in [0, 0.05]$. In Figs. 3 and 4, we use markers to indicate values of ε in increments of $10 \times \Delta\varepsilon = 0.01$ to "guide the eye."

In Fig. 3 we show the real and imaginary parts of the fundamental quadrupolar quasinormal frequency as a function of ε and normalized with respect to its value in general relativity, i.e.,

$$\delta\mathrm{Re}\omega_{\ell n}^{(\pm)}(\varepsilon) = \frac{\mathrm{Re}\omega_{\ell n}^{(\pm)}(\varepsilon)}{\mathrm{Re}\omega_{\ell n}^{(\pm)}(0)}, \qquad \delta\mathrm{Im}\omega_{\ell n}^{(\pm)}(\varepsilon) = \frac{\mathrm{Im}\omega_{\ell n}^{(\pm)}(\varepsilon)}{\mathrm{Im}\omega_{\ell n}^{(\pm)}(0)}.$$

The top and bottom panels show our results for these two quantities, respectively. The solid curves are the results of our phase-amplitude calculation. We use the markers to
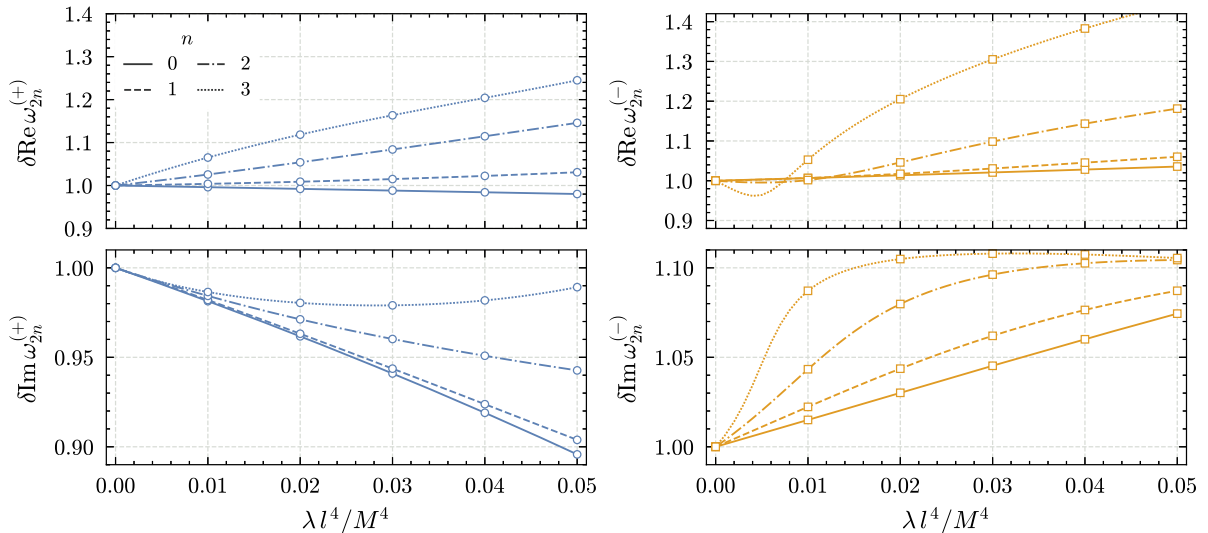

FIG. 4. The quadrupolar polar- and axial-parity quasinormal frequencies, normalized with respect to their Schwarzschild values, as functions of $\varepsilon = \lambda l^4/M^4$. The left and right columns correspond to quasinormal modes of polar and axial parities, respectively, whereas the top and bottom panels show the real and imaginary parts. The line styles indicate different overtone numbers n. We see that the deviations from the general-relativistic values can become nonmonotonic as we increase the value of ε. We also find that the curves become nonlinear for smaller values of ε the higher the overtone number n.

distinguish the curves corresponding to quasinormal modes of polar (+) and axial (−) parities, which are no longer the same. We also show, with the dashed curves, the fits obtained in Ref. [36]; cf. Table III therein. These fits are a linear approximation to the behavior of $\omega_{20}^{(\pm)}$ with respect to ε, which does become nonlinear as ε growth; cf. Ref. [34], Fig. 1. The same behavior can be seen here. In addition, our results are in excellent agreement with the linear fits of Ref. [36] for $\varepsilon \lesssim 0.03$ and across the whole ε range for $\delta\mathrm{Re}\omega_{20}^{(+)}$ and $\delta\mathrm{Im}\omega_{20}^{(-)}$. The agreement is quite remarkable considering that we do not integrate the same set of perturbations equations and that we use different numerical techniques to compute the quasinormal modes; recall Sec. III. We find a similar level of agreement for the fundamental $\ell = 3$ quasinormal mode frequency. As a consequence, our numerical results are also in agreement with those of de Rham *et al.* [33].

We also briefly studied the case where ε is negative. For sufficiently small values of $|\varepsilon|$, we would expect that the deviations from the quasinormal frequencies in general relativity to be equal in magnitude, but with an opposite sign relative to the case where ε is positive. We found that this was indeed the case for $\omega_{20}^{(\pm)}$.

2. Overtones and the limits of the effective field theory

With confidence built on the applicability of the phase-amplitude approach to our problem and on our numerical code, we now investigate, for the first time, the dependence of the overtones as a function of ε.

In Fig. 4 we show $\omega_{2n}^{(\pm)}$ as a function of ε. Panels on the left and right columns show the polar (+) and axial (−) quasinormal frequencies, respectively. We show their real and imaginary parts (normalized with respect to their values in general relativity) in the top and bottom rows, respectively. Different line styles represent different overtone numbers n as indicated in the legend in the top-left panel. We observe that as the overtone number n increases, the smaller the range of ε at which the scaling is linear. Moreover the curves do not necessarily behave monotonically with respect to ε. This can best be seen for the $n = 3$ axial-parity quasinormal-mode frequency. These conclusions are shared among the overtones associated to $\ell = 2, 3$ and 4. The emerging picture has two facets: (i) *overtones are more sensitive to the EFT corrections than the fundamental mode*, and (ii) *the maximum value of ε above which the linear approximation breaks down depends on ℓ and n.*

In order to discuss the behavior of the quasinormal-mode frequencies, we first describe the regime of applicability of the EFT of gravity. As already mentioned, the EFT corrections can be computed in powers of ε, with the EFT breaking down once $\varepsilon \simeq \varepsilon_{\mathrm{th}}$ where $\varepsilon_{\mathrm{th}}$ is a threshold value of order 1. This is the statement that the black-hole curvature radius has to be larger than the scale l. Moreover,

one also needs the frequency of perturbations not too large. At fixed ℓ, increasing n corresponds in increasing the proper frequency $f_{\ell n}$ of the quasinormal modes. The quantity $f_{\ell n}$ can be identified with the real part of $\omega_{\ell n}/(2\pi)$ only if $\mathrm{Re}\omega_{\ell n} \gg \mathrm{Im}\omega_{\ell n}$. Typically this is not the case for the Schwarzschild quasinormal modes and, following Ref. [72], one has to make the following identification in order to have a monotonically increasing spectrum of proper frequencies

$$f_{\ell n} = (2\pi)^{-1}[\mathrm{Re}\omega_{\ell n}^2 + \mathrm{Im}\omega_{\ell n}^2]^{1/2}. \qquad (63)$$

Then, at fixed ε, an overtone with proper frequency $f_{\ell n}$ can be described within the EFT provided that [73]

$$\varepsilon_f = \lambda(lf_{\ell n})^4 = \varepsilon(Mf_{\ell n})^4 \ll \varepsilon^{-1}. \qquad (64)$$

The condition above is the statement that the covariant contraction $k^\mu\kappa_\mu \ll l^{-2}$, where k^μ and κ^μ are respectively the typical four-momenta of the gravitational perturbations and of the black hole background. The latter can be defined as the normalized covariant derivative of the Kretschmann scalar [73].

After these considerations, let us discuss the behavior we find for the quasinormal modes. Our results show a growing impact of the EFT corrections on $\omega_{\ell n}$ as n increases at a fixed multipole ℓ; see the "bird's-eye view" shown in Fig. 5. Reasoning in terms of Eq. (63) offers a qualitative explanation for this behavior. Overtones correspond to high-frequency waves and consequently probe deeper the effective potential which is fixed by ε and ℓ. As a consequence, overtones are more sensitive to changes to the effective potential that occur near the black-hole horizon, which is the case in our problem—recall Fig. 1. Complementary, let us also remark that this behavior is a general feature of perturbation theory when the correction to the potential comes from regions far from the potential peak, or the potential minimum in the bound-problem case. An example in quantum mechanics is given by a harmonic oscillator potential $V(x) \propto x^2$ in the presence of a small anharmonicity (going as, e.g., $\delta V(x) \propto x^4$). At first order in perturbation theory, the corrections to the nth eigenenergy grow as n to some given power (see for example Ref. [74]). In our case, the EFT corrections grow toward the horizon while the peak of the unperturbed potential is approximately at the light ring and we therefore expect a similar behavior.

The nonlinear behavior above a certain $\varepsilon_{\mathrm{max}}$ of the quasinormal frequencies sets an upper limit on the linear description of our problem, and indicates that higher powers of ε are necessary to describe the regime for $\varepsilon \gtrsim \varepsilon_{\mathrm{max}}$. This means that we either need to go to second order in perturbation theory (our perturbations equations are linear in the metric perturbations and in ε) or that we need to include higher-order operators in our starting action (1). At
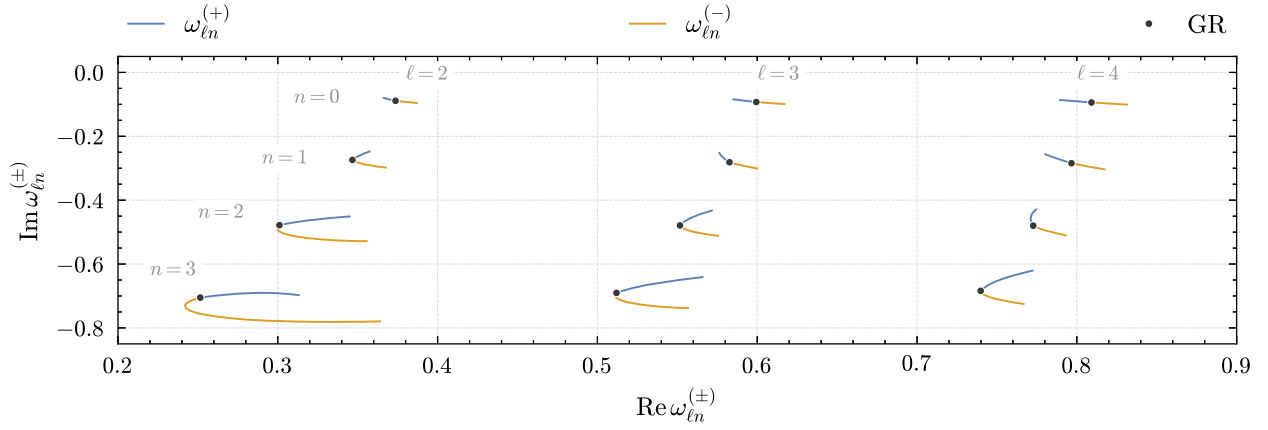
FIG. 5. The spectrum of quasinormal modes $\omega_{\ell n}^{(\pm)}$ in the complex plane in the range $\varepsilon \in [0, 0.05]$. The circles mark the location of the general-relativity ("GR") quasinormal mode frequencies, that are coincident for axial and polar modes. A nonzero value of the EFT parameter ε breaks this symmetry, and axial- and polar-parity frequencies flow along the blue and orange colored lines, respectively, as we increase ε. The larger the overtone number n, the farther away the quasinormal frequencies, at fixed multipole number ℓ, with respect to the fundamental mode, $n = 0$.

second order in perturbation theory the second-order quasinormal frequencies are a sum of first-order quasinormal frequencies [75,76]; see, e.g., Refs. [77–83] for further details. As a consequence, we expect the second-order quasinormal frequencies to also scale with ε in the EFT. Assuming that all the dimensionless factors entering in the higher-dimension operators of the EFT are numbers of order one, which is technically natural [31], then the effects from dimension-eight operators would be of order $\varepsilon^{3/2}$. Hence, they would be the dominant contribution to the quasinormal frequencies in the nonlinear regime of ε.

From these results and considerations, we find that the onset of the nonlinear behavior in the quasinormal-mode frequencies is best characterized in terms of the parameter ε_f, rather than ε. In Fig. 6 we show, for each ℓ and n, the value of $\varepsilon_f^{1/4}$ at which nonlinear corrections start appearing.

FIG. 6. Values of $\varepsilon_f^{1/4}$ at which a given quasinormal frequency deviates by more than 20% from its linear fit in ε. Polar $(+)$ and axial $(-)$ quasinormal modes are shown on the left and right panels, respectively. Notice that the values of $\varepsilon_f^{1/4}$ in the tables vary only by a factor of two between different modes.

More specifically, we first evaluate the value of ε at which $\omega_{\ell n}^{(\pm)}$ deviates from its linear fit by more than 20%. This gives us values of $\varepsilon_{\max}$ and $\omega_{\ell n,\max}^{(\pm)} = \omega_{\ell n}^{(\pm)}(\varepsilon_{\max})$ associated to this mode *and* threshold value. For instance, for $\omega_{20}^{(\pm)}$ we find $\varepsilon_{\max} > 0.05$, hence all values of ε considered by us are interpreted to be within the linearized regime according to this criteria. In this case, we take for $\omega_{\ell n,\max}^{(\pm)}$ the value of $\omega_{\ell n}^{(\pm)}$ at $\varepsilon = 0.05$. However, in general, this is not what happens for other values of ℓ and n. Then, with the values of $\varepsilon_{\max}$ and $\omega_{\ell n,\max}^{(\pm)}$ in hand, we can compute the respective value of ε_f using Eq. (64). The values obtained are below one, meaning that the onset of nonlinearities appears below the breaking of the EFT, as one would expect.

As mentioned above, for values of both ε and ε_f close to unity the EFT description inevitably breaks down: it is not enough to include higher-order operators and any prediction can only be made with an ultraviolet (UV) completion of the EFT. As explained in Ref. [31], assuming a *soft UV completion*, the corrections to the quasinormal-mode frequencies (and other observable quantities) are expected to saturate after the breaking of the EFT. In Fig. 7 we give a schematic representation of the behavior of $f_{\ell n}$ in this scenario; see also Fig. 1 of Ref. [42] and related discussion therein.

At this point it is clear that the condition in Eq. (64) is necessarily violated for sufficiently large n, given a value of ε. In other words the EFT *cannot describe all overtones*. Using the asymptotic behavior of the Schwarzschild quasinormal frequencies in general relativity we can get a good estimate for this maximum value of n, that we call $n_{\max}$. The spectrum at large n is independent on ℓ and is given by

$$M\omega_{\ell n} \simeq (8\pi)^{-1} \log 3 - \mathrm{i}(n + 1/2)/4, \quad \text{as } n \to \infty. \quad (65)$$
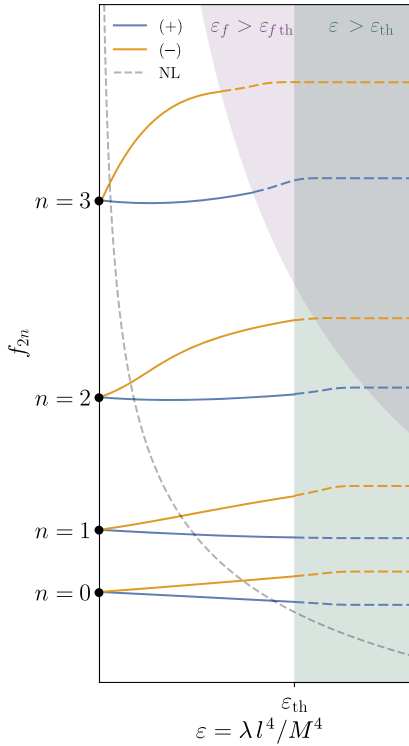
FIG. 7. Schematic representation of the quadrupolar quasinormal proper frequencies f_{2n} for even (blue) and odd (orange) parities, as functions of ε and the regions of validity of the EFT calculation. For small ε, deviations from the GR values are approximately linear. The onset of nonlinearities in the corrections is represented by the gray dashed line (NL): above this line one needs to include higher-order contributions in ε. When $\varepsilon \gtrsim \varepsilon_{\rm th} \sim \mathcal{O}(1)$ (green-shaded area) or $\varepsilon_f \gtrsim \varepsilon_{f\rm th} \sim \varepsilon^{-1}$ (purple-shaded area) the EFT description breaks down and one has to resort to its UV completion to make predictions; see the discussion around Eq. (64). Under the assumption of a soft UV completion, the corrections to the quasinormal frequencies are expected to saturate, as illustrated with the dashed lines.

See Refs. [69,84] for numerical studies in this limit and Refs. [85–88] for the posterior analytical derivations of this result. Using this expression, Eqs. (63) and (64), and imposing the latter as an equality, we readily obtain

$$n_{\rm max} \simeq (8\pi)/\sqrt{\varepsilon} - 1/2 + \mathcal{O}(\sqrt{\varepsilon}). \qquad (66)$$

The value we obtained is quite large even for ε close to unity, $n_{\rm max} \sim \mathcal{O}(25)$. Corrections not captured by the EFT are bound to appear below, or at most at, $n_{\rm max}$.

B. The quasinormal-mode excitation factors

1. Code validation and comparison with the literature in the limit of general relativity

To our knowledge this is the first time that quasinormal-mode excitation factors have been computed for black-hole

solutions in a theory that is not general relativity. To validate our numerical results in the limit of general relativity we performed two tests.

First, in general relativity, the excitation factors of polar and axial quasinormal modes are related as

$$B_{\ell n}^{(+)} = \frac{2\lambda_\ell(\lambda_\ell + 1) + 6iM\omega_{\ell n}}{2\lambda_\ell(\lambda_\ell + 1) - 6iM\omega_{\ell n}} B_{\ell n}^{(-)}, \qquad (67)$$

as shown by Leaver [11]. This relation follows from two identities relating the transmission and reflection coefficients of the Zerilli and Regge-Wheeler functions found by Chandrasekhar and Detweiler [8]. We note that despite sharing the same quasinormal mode spectra, the Zerilli and Regge-Wheeler modes have different excitation factors. As a consistency check of our code, we verified that our numerical calculations of $B_{\ell n}^{(\pm)}$ satisfy Eq. (67) with a mean error of approximately $\mathcal{O}(10^{-5})$ across the ℓn-parameter space we studied. This error decreases by one order of magnitude if we exclude the $n = 3$ overtones.

As a second test, we compared our values of $B_{\ell n}^{(\pm)}$ with those obtained by Zhang, Berti, and Cardoso [18] (see Table II therein), who employed the formalism of Mano, Suzuki, and Takasugi [89–91]. This scheme is based on a matched asymptotic expansion between a Coulomb-series expansion near spatial infinity and a series expansion involving hypergeometric functions near the event horizon. Reassuringly, we find excellent agreement between our phase-amplitude-based calculation and those of Ref. [18]. For example, for the excitation factors of the fundamental quadrupole quasinormal frequencies we have

$$B_{20}^{(+)} = 0.120928 + 0.0706657i, \qquad (68a)$$

$$B_{20}^{(+)} = 0.120923 + 0.0706696i, \qquad (68b)$$

for the polar-parity mode and

$$B_{20}^{(-)} = 0.126902 + 0.0203152i, \qquad (69a)$$

$$B_{20}^{(-)} = 0.126902 + 0.0203152i, \qquad (69b)$$

for the axial-parity mode. In each of the two foregoing equations the second line is taken from Ref. [18], Table II.

2. Effective-field-theory corrections to the excitation coefficients

As we observed for the quasinormal-modes frequencies, we also find that the associated excitation factors vary more with respect to their values in general relativity, as functions of ε, for the overtones. As an example, we show in Fig. 8 the trajectories in the complex plane of the quadrupolar quasinormal mode excitation factors as we increase ε from zero (circles) to 0.05. Solid and dashed lines correspond to
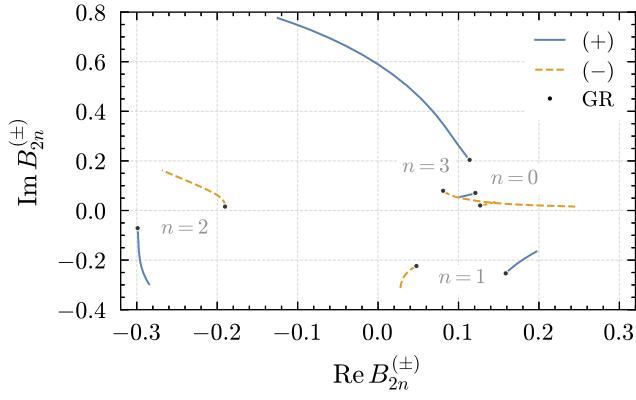
FIG. 8.   Quadrupolar quasinormal mode excitation factors $B_{2n}^{(\pm)}$ in the range $\varepsilon \in [0, 0.05]$. The circles mark the limit of general relativity. Solid and dashed lines correspond to the excitation factors of the quasinormal modes of polar and axial parities, respectively. The labels indicate the pairs of curves that are associated to each overtone number n. We see that the excitation factors move farther away from their general-relativistic values the larger the overtone number. The same behavior occurs for the higher multipoles ℓ we studied.

the excitation factors of the quasinormal modes of polar and axial parities, respectively. Pairs of curves belonging to the same overtone number n are indicated by the labels. We found the same qualitative behavior for higher multipoles ℓ. We present some sample values of the excitation factors in Table I.

3. The effective quasinormal mode amplitude

As an application of the calculations presented in this section, we perform a preliminary analysis of the gravitational wave amplitude associated with the polar and axial quasinormal modes. In practice this is done by introducing an "effective" amplitude related to the magnitude of the Green's function used in the solution of the radial perturbation equations for a given set of initial data; see, e.g., Ref. [16]. The relevant part of the Green's function is the one describing the quasinormal mode ringdown signal and is given by $h = A_{\text{out}}(\omega_n)/\alpha_n$ for each individual mode ω_n. The effective amplitude is then $h_{\text{eff}} = \sqrt{N}h$, where $N = \sqrt{\text{Re}\omega_n/\text{Im}\omega_n}$ is the number of cycles in the
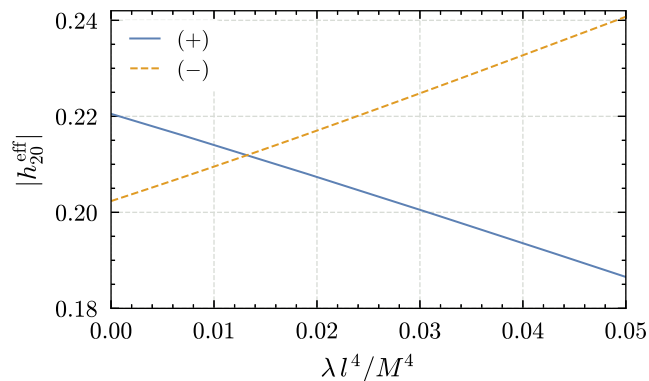
TABLE I.   Quasinormal-mode excitation factors of the Zerilli and Regge-Wheeler functions for a selection of multipoles ℓ overtones n numbers and $\varepsilon = \lambda l^4/M^4 = 0$, 0.01 and 0.02. Our results in the limit of general relativity, $\varepsilon = 0$, are in excellent agreement with the calculations of Ref. [18].

$B_{\ell n}^{(+)}$	$\varepsilon(\times 10^{-2})$	$\ell = 2$	$\ell = 3$	$\ell = 4$
	0	$0.120928 + 0.0706657i$	$-0.0889688 - 0.0611773i$	$0.0621245 + 0.069099i$
$n = 0$	1	$0.117708 + 0.0672479i$	$-0.087801 - 0.0568295i$	$0.0628948 + 0.0644908i$
	2	$0.11423 + 0.0639308i$	$-0.0863858 - 0.0524486i$	$0.0634276 + 0.0597634i$
	0	$0.158645 - 0.253326i$	$-0.191931 + 0.264798i$	$0.279718 - 0.24183i$
$n = 1$	1	$0.164761 - 0.235166i$	$-0.183766 + 0.246502i$	$0.259492 - 0.229203i$
	2	$0.171749 - 0.217066i$	$-0.176498 + 0.227387i$	$0.239777 - 0.215239i$
	0	$-0.298938 - 0.0711347i$	$0.43677 + 0.20459i$	$-0.543165 - 0.478076i$
$n = 2$	1	$-0.298122 - 0.115973i$	$0.394863 + 0.230675i$	$-0.478737 - 0.464904i$
	2	$-0.297456 - 0.16154i$	$0.353727 + 0.258994i$	$-0.413138 - 0.455013i$
	0	$0.11382 + 0.204126i$	$-0.000943158 - 0.476399i$	$-0.374548 + 0.859556i$
$n = 3$	1	$0.0959369 + 0.280675i$	$0.0877723 - 0.47838i$	$-0.456808 + 0.756741i$
	2	$0.076331 + 0.367397i$	$0.177021 - 0.481374i$	$-0.542232 + 0.6564i$

$B_{\ell n}^{(-)}$	$\varepsilon(\times 10^{-2})$	$\ell = 2$	$\ell = 3$	$\ell = 4$
	0	$0.126902 + 0.0203152i$	$-0.0938897 - 0.0491928i$	$0.0653479 + 0.0652391i$
$n = 0$	1	$0.130744 + 0.0222580i$	$-0.095795 - 0.0519542i$	$0.0659238 + 0.0680835i$
	2	$0.134644 + 0.0251759i$	$-0.097599 - 0.0548384i$	$0.0664031 + 0.0709206i$
	0	$0.0476827 - 0.223755i$	$-0.151135 + 0.269749i$	$0.261488 - 0.251524i$
$n = 1$	1	$0.0389361 - 0.242548i$	$-0.154331 + 0.289785i$	$0.274625 - 0.268574i$
	2	$0.0330242 - 0.262936i$	$-0.159411 + 0.309949i$	$0.289045 - 0.284968i$
	0	$-0.190283 + 0.0157516i$	$0.415029 + 0.141039i$	$-0.549216 - 0.435328i$
$n = 2$	1	$-0.199520 + 0.0607662i$	$0.458619 + 0.108671i$	$-0.619525 - 0.434249i$
	2	$-0.219544 + 0.0942148i$	$0.506304 + 0.0827037i$	$-0.69088 - 0.439270i$
	0	$0.0808586 + 0.0796019i$	$-0.0434027 - 0.412748i$	$-0.316922 + 0.837911i$
$n = 3$	1	$0.130958 + 0.0353271i$	$-0.138089 - 0.418874i$	$-0.217410 + 0.944489i$
	2	$0.173338 + 0.0240910i$	$-0.220413 - 0.444001i$	$-0.131563 + 1.05946i$

FIG. 9. The effective quasinormal mode amplitude for the fundamental quadrupolar quasinormal modes of axial (−) and polar (+) parities as a functions of $\varepsilon = \lambda l^4/M^4$. For $\varepsilon \lesssim 0.012$, the amplitude is largest for the for polar quasinormal mode. A crossover occurs around $\varepsilon \approx 0.012$, above which the amplitude of the axial quasinormal mode becomes larger.

ringdown signal; this obviously assumes a weakly damped mode. Therefore, the effective signal amplitude of each polar and axial quasinormal mode $\omega_{\ell n}$ is given by

$$h_{\ell n}^{(\pm),\mathrm{eff}} = 2 \left[\frac{\mathrm{Re}\,\omega_{\ell n}^{(\pm)}}{\mathrm{Im}\,\omega_{\ell n}^{(\pm)}} \right]^{\frac{1}{2}} \omega_{\ell n}^{(\pm)} B_{\ell n}^{(\pm)}, \qquad (70)$$

that we can compute with the numerical data obtained in the previous section.

In Fig. 9 we show the effective amplitudes of the fundamental quasinormal modes of polar (solid line) and axial (dashed line) parities as functions of ε. We see that the "polar-wave amplitude" dominates over its axial counterpart for $\varepsilon \lesssim 0.012$, above which the axial mode dominates. This suggests that *at least for some initial data* (see the "asymptotic approximation" of Ref. [92]) that the dominant contribution to the gravitational-wave ringdown amplitude comes from the polar perturbations conditional, naturally, also on the cutoff $\varepsilon_{\max}$ for the onset on nonlinearities.

The dependence on this statement on the initial data (or source of perturbation) can be seen from source-dependent term in the quasinormal-mode excitation amplitude (45). As an extreme example, it suffices to recall that $I_n^{(-)}$ vanishes for a test particle radially infalling into a Schwarzschild black hole even if $B_n^{(-)}$ is nonzero. Therefore, quasinormal modes of axial parity are not excited in this situation. Nonetheless, we note that previous works in general relativity for plunging test particles [93] and in the close-limit approximation [94] do find that the amplitude associated to perturbations of polar parity to be larger than those of axial parity. We conjecture that this will also be the case in the EFT studied here.

VI. CONCLUSIONS AND OUTLOOK

Motivated by a dearth of understanding about the quasinormal spectrum and about how these quasinormal modes are excited in extensions to general relativity, we reexamined and extended previous literature on perturbations of nonrotating black holes in an EFT of general relativity. Using a "quick and dirty" phase-amplitude method [37], we computed both the first quasinormal-frequency overtones and the quasinormal-mode excitation factors. We found that the overtone frequencies (and their respective excitation factors) are more sensitive than the fundamental quasinormal modes to the length scale l introduced by the higher-derivative operators in the EFT. We interpreted these results from an EFT perspective, and identified the domain of validity of the EFT description; see Fig. 7. We also suggested the existence of an upper bound on the overtone number n, above which a UV completion of the EFT becomes necessary to fully characterize the black hole's quasinormal mode spectrum. In addition, we presented a simple explanation for the inequivalence between the spectra of quasinormal modes of polar and axial parities in the EFT.

Let us put our findings in perspective. In Sec. V we argued that the overtones can be interpreted as high-frequency perturbations [72], and hence they probe the structure of the black-hole effective potential region near the horizon. This is the region of spacetime where the EFT corrections are most significant; this is unsurprising given that the EFT introduces higher powers of the curvature that become relevant near the horizon. Following this reasoning, it is not unreasonable to conjecture that this *sensitivity of the overtones to new length scales would also be seen in other theories that involve higher-curvature corrections to general relativity, including those that introduce couplings to extra degrees of freedom.*[6]

It is also tempting to interpret our results in terms of an instability of the quasinormal-mode spectrum induced by the higher-derivative operators in the EFT. In the language of Jaramillo *et al.* [96], this would correspond to an instability of the overtones; see, e.g., Refs. [15,97,98] for earlier related works. Confirmation of this interpretation would require an analysis of the quasinormal pseudospectrum associated to Eq. (15) following, e.g., Ref. [96]. If confirmed, it would suggest that the *instability of the overtones is a general expectation from an EFT perspective.* It would then be interesting to understand how this ties with our conclusion that one cannot describe the quasinormal-mode spectrum past a certain overtone number without invoking the UV completion of the EFT.

Our calculation of the quasinormal-mode excitation factors and the observation that those associated to overtone are *also* sensitive to the near-horizon modifications induced by the EFT has implications to the signatures of these corrections in gravitational-wave observations. We presented a first, but limited, analysis focusing on the

---

[6]While this paper was being completed, a preprint presented the same reasoning [95].

implications of isospectrality breaking in Sec. V (see Fig. 9), but more work is evidently needed [99].

APPENDIX A: DERIVATION OF THE BLACK HOLE SOLUTION

To obtain the black-hole spacetime described by the line element (6), we solve the field equations (4) perturbatively in ε. To do so, we take N and f to be deformations away from their Schwarzschild expressions:

$$f = 1 - 2\bar{M}/r + \varepsilon \delta f, \tag{A1a}$$

$$N = 1 + \varepsilon \delta N, \tag{A1b}$$

where $\bar{M}$ is a positive constant, $\varepsilon = \lambda l^4/\bar{M}^4$, and δf and δN are functions of r. From the tt and rr components of field equations, we find that δN and δf obey the decoupled first-order differential equations:

$$\left(\frac{\mathrm{d}}{\mathrm{d}r} + \frac{1}{r}\right)\delta f = \frac{1080}{r}\frac{\bar{M}^6}{r^6} - \frac{2352}{r}\frac{\bar{M}^7}{r^7}, \tag{A2a}$$

$$\frac{\mathrm{d}(\delta N)}{\mathrm{d}r} = \frac{648}{r}\frac{\bar{M}^6}{r^6}. \tag{A2b}$$

The solutions of these equations are

$$\delta f = \frac{c_1}{r} + \frac{216\bar{M}^6}{r^6} - \frac{392\bar{M}^7}{r^7}, \tag{A3a}$$

$$\delta N = c_2 - \frac{108\bar{M}^6}{r^6}, \tag{A3b}$$

where c_1 and c_2 are integration constants. They can be fixed by examining the far-field expansion of $g_{tt} = -N^2 f$,

$$-g_{tt} \simeq 1 + 2\varepsilon c_2 - [2\bar{M} - \varepsilon(c_1 - 4\bar{M}c_2)]/r. \tag{A4}$$

We can then set $c_2 = 0$, as it amounts to a shift in the time coordinate t. From the r^{-1} term, we identify the ADM mass of the spacetime to be

$$M = \bar{M} - \varepsilon c_1/2. \tag{A5}$$

Hence, the bare mass $\bar{M}$ is renormalized by the dimension-six operators in the action. We now solve Eq. (A5) for $\bar{M}$, noticing that $\varepsilon = \lambda l^4/\bar{M}^4 = \lambda l^4/M^4$ to $\mathcal{O}(\varepsilon)$. The result is $\bar{M} = M + \varepsilon c_1/2$, which substituted together with $c_2 = 0$ in Eqs. (A3) and (A1), results in Eq. (7) to $\mathcal{O}(\varepsilon)$.

APPENDIX B: THE PETROV CLASSIFICATION OF THE BLACK HOLE SOLUTION

The Petrov type of a spacetime can be identified by constructing a null tetrad l^μ, n^μ, m^μ and its complex conjugate $\bar{m}^\mu$ and computing the Newman-Penrose scalars. The tetrad satisfies the normalization $l^\mu n_\mu = -1$, $m^\mu \bar{m}_\mu = 1$ with all the other contractions set to vanish. In this Appendix, we follow Refs. [106,107] to determine the Petrov type of the black hole solution given by Eqs. (6) and (13).

When the spacetime is algebraically special (having at least one degenerate principal null direction), the following condition is satisfied

$$I^3 = 27J^2, \tag{B1}$$

where

$$\begin{aligned}
I &= \frac{1}{2}\tilde{C}_{\alpha\beta\gamma\delta}\tilde{C}^{\alpha\beta\gamma\delta}, \\
&= 3\Psi_2^2 - 4\Psi_1\Psi_3 + \Psi_4\Psi_0, \tag{B2}
\end{aligned}$$

$$\begin{aligned}
J &= -\frac{1}{6}\tilde{C}_{\alpha\beta\gamma\delta}\tilde{C}^{\gamma\delta}{}_{\mu\nu}\tilde{C}^{\mu\nu\alpha\beta}, \\
&= -\Psi_2^3 + 2\Psi_1\Psi_3\Psi_2 + \Psi_0\Psi_4\Psi_2 - \Psi_4\Psi_1^2 - \Psi_0\Psi_3^2, \tag{B3}
\end{aligned}$$

where we defined

$$\tilde{C}_{\alpha\beta\gamma\delta} = \frac{1}{4}\left(C_{\alpha\beta\gamma\delta} + \frac{i}{2}\epsilon_{\alpha\beta\mu\nu}C^{\mu\nu}{}_{\gamma\delta}\right), \tag{B4}$$

for a Weyl tensor $C_{\alpha\beta\gamma\delta}$, Levi-Civita tensor $\epsilon_{\alpha\beta\mu\nu}$, and where Ψ_i are the Newman-Penrose Weyl scalars with the only restriction of $\Psi_4 \neq 0$:

$$\Psi_0 = C_{\alpha\beta\gamma\delta}l^\alpha m^\beta l^\gamma m^\delta, \tag{B5a}$$

$$\Psi_1 = C_{\alpha\beta\gamma\delta}l^\alpha n^\beta l^\gamma m^\delta, \tag{B5b}$$

$$\Psi_2 = C_{\alpha\beta\gamma\delta}l^\alpha m^\beta \bar{m}^\gamma n^\delta, \tag{B5c}$$

$$\Psi_3 = C_{\alpha\beta\gamma\delta}l^\alpha n^\beta \bar{m}^\gamma n^\delta, \tag{B5d}$$

$$\Psi_4 = C_{\alpha\beta\gamma\delta}n^\alpha \bar{m}^\beta n^\gamma \bar{m}^\delta. \tag{B5e}$$

In particular, I and J are nonvanishing for Petrov type D (and II).

To further determine the Petrov type, we study the following relations that are invariant under a tetrad rotation and hold for type D (and III):

$$K = 0, \qquad N - 9L^2 = 0, \qquad (B6)$$

where

$$K = \Psi_1 \Psi_4^2 - 3\Psi_4 \Psi_3 \Psi_2 + 2\Psi_3^3, \qquad (B7a)$$

$$L = \Psi_2 \Psi_4 - \Psi_3^2, \qquad (B7b)$$

$$N = \Psi_4^3 \Psi_0 - 4\Psi_4^2 \Psi_1 \Psi_3 + 6\Psi_4 \Psi_2 \Psi_3^2 - 3\Psi_3^4. \qquad (B7c)$$

To summarize, the spacetime is type D if Eqs. (B1) and (B6) are satisfied for nonvanishing I and J.

Let us now apply the above formulation to the black hole solution described by Eqs. (6) and (13). One of the simplest null tetrad is found as

$$l^\mu = \left[\frac{r}{r - r_{\rm h}}, 1 - \frac{5}{8}\frac{M}{r}\varepsilon\left(1 + \frac{2M}{r} + \frac{4M^2}{r^2} + \frac{8M^3}{r^3} + \frac{16M^4}{r^4} - \frac{704}{5}\frac{M^5}{r^5}\right), 0, 0\right] + \mathcal{O}(\varepsilon^2), \qquad (B8a)$$

$$n^\mu = \left[\frac{3r - r_{\rm h}}{2(r - r_{\rm h})} + \frac{5}{16}\frac{M}{r}\varepsilon\left(1 + \frac{2M}{r} + \frac{4M^2}{r^2} + \frac{8M^3}{r^3} + \frac{16M^4}{r^4} + \frac{32M^5}{r^5}\right),\right.$$
$$\left.\frac{r + r_{\rm h}}{2r} - \frac{5}{8}\frac{M}{r}\varepsilon\left(1 + \frac{2M}{r} + \frac{4M^2}{r^2} + \frac{8M^3}{r^3} + \frac{16M^4}{r^4} - \frac{272}{5}\frac{M^5}{r^5} - \frac{864}{5}\frac{M^6}{r^6}\right), \frac{\sqrt{2}}{r}, 0\right] + \mathcal{O}(\varepsilon^2), \qquad (B8b)$$

$$m^\mu = \left[\frac{r}{r - r_{\rm h}}, 1 - \frac{5}{8}\frac{M}{r}\varepsilon\left(1 + \frac{2M}{r} + \frac{4M^2}{r^2} + \frac{8M^3}{r^3} + \frac{16M^4}{r^4} - \frac{704}{5}\frac{M^5}{r^5}\right), \frac{1}{\sqrt{2}r}, \frac{i}{\sqrt{2}r\sin\theta}\right] + \mathcal{O}(\varepsilon^2). \qquad (B8c)$$

Here, at $\mathcal{O}(\epsilon)$, we substituted $r_{\rm h} = 2M$ to simplify the expressions. We checked that the Petrov type of the black hole does not change even if we leave $r_{\rm h}$ arbitrary. Then, using Eqs. (B5) and (B8), we find that Ψ_i are given by

$$\Psi_0 = \Psi_1 = \mathcal{O}(\varepsilon^2), \qquad (B9a)$$

$$\Psi_2 = \frac{r_{\rm h}}{2r^3} + \frac{5M}{16r^3}\varepsilon\left(1 - \frac{2304M^5}{5r^5} + \frac{960M^6}{r^6}\right) + \mathcal{O}(\varepsilon^2), \qquad (B9b)$$

$$\Psi_3 = 3\Psi_2, \qquad \Psi_4 = 6\Psi_2. \qquad (B9c)$$

We can now obtain the Petrov type of the black hole. First, the Weyl scalar invariants I and J are given by

$$I = \frac{3r_{\rm h}^2}{4r^6} + \frac{15M^2}{8r^6}\varepsilon\left(1 - \frac{2304M^5}{5r^5} + \frac{960M^6}{r^6}\right) + \mathcal{O}(\varepsilon^2), \qquad (B10a)$$

$$J = -\frac{r_{\rm h}^3}{8r^9} - \frac{15M^3}{16r^9}\varepsilon\left(1 - \frac{2304M^5}{5r^5} + \frac{960M^6}{r^6}\right) + \mathcal{O}(\varepsilon^2), \qquad (B10b)$$

which leads to

$$I^3 - 27J^2 = \mathcal{O}(\varepsilon^2). \qquad (B11)$$

Second, K, L, and N are given by

$$K = \mathcal{O}(\varepsilon^2), \qquad (B12a)$$

$$L = -\frac{3r_{\rm h}^2}{4r^6} - \frac{15M^2}{8r^6}\varepsilon\left(1 - \frac{2304M^5}{5r^5} + \frac{960M^6}{r^6}\right) + \mathcal{O}(\varepsilon^2), \qquad (B12b)$$

$$N = \frac{81r_{\rm h}^4}{16r^{12}} + \frac{405M^4}{4r^{12}}\varepsilon\left(1 - \frac{2304M^5}{5r^5} + \frac{960M^6}{r^6}\right) + \mathcal{O}(\varepsilon^2), \qquad (B12c)$$

which leads to

$$N - 9L^2 = \mathcal{O}(\varepsilon^2). \qquad (B13)$$

Thus, to the order we worked on, I and J are nonvanishing and Eqs. (B1) and (B6) are satisfied, so the spacetime is of Petrov type D.

APPENDIX C: DERIVATION OF EQ. (13)

Let us derive Eq. (13b) first. We start by adding and subtracting $r_{\rm h}/r$ to Eq. (10) and collect the terms as,

$$f^{-1} = \left[1 - \frac{r_{\rm h}}{r} + \left(\frac{r_{\rm h} - 2M}{r} + \varepsilon\delta f\right)\right]^{-1}. \qquad (C1)$$

From Eq. (9) we see that $r_h - 2M$ is of order ε

$$r_h - 2M = \varepsilon \delta r_h = -\frac{5}{8} \varepsilon M. \tag{C2}$$

We can then rewrite Eq. (C1), by factoring out $1 - r_h/r$:

$$f^{-1} = \left(1 - \frac{r_h}{r}\right)^{-1} \left[1 + \varepsilon \frac{\delta r_h/r + \delta f}{1 - r_h/r}\right]^{-1},$$

$$\simeq \left(1 - \frac{r_h}{r}\right)^{-1} \left[1 - \varepsilon \frac{\delta r_h/r + \delta f}{1 - 2M/r}\right], \tag{C3}$$

where we replaced r_h/r by its $\mathcal{O}(\varepsilon^0)$ value in the second line. We now use the explicit forms of δr_h and δf, given in Eqs. (11) and (C2), to find

$$f^{-1} = \left(1 - \frac{r_h}{r}\right)^{-1} \left[1 - \varepsilon \left(1 - \frac{2M}{r}\right)^{-1} \left(-\frac{5}{8} \frac{M}{r}\right.\right.$$

$$\left.\left. + \frac{216M^6}{r^6} - \frac{392M^7}{r^7}\right)\right]. \tag{C4}$$

Although not evident, the term proportional to ε inside the square brackets is regular at $r = 2M$, with value $-3/2$. To see this explicitly, we use the factorization

$$-\frac{5}{8} \frac{M}{r} + \frac{216M^6}{r^6} - \frac{392M^7}{r^7}$$

$$= -\left(1 - \frac{2M}{r}\right) \left(\frac{5}{8} \frac{M}{r} + \frac{5}{4} \frac{M^2}{r^2} + \frac{5}{2} \frac{M^3}{r^3}\right.$$

$$\left. + \frac{5M^4}{r^4} + \frac{10M^5}{r^5} - \frac{196M^6}{r^6}\right). \tag{C5}$$

Using this result, we obtain Eq. (13b). Equation (13a) is derived in the same manner. We find

$$N^2 f = \left(1 - \frac{r_h}{r}\right) \left[1 + 2\varepsilon \delta N + \varepsilon \frac{\delta r_h/r + \delta f}{1 - 2M/r}\right],$$

$$= \left(1 - \frac{r_h}{r}\right) \left[1 - \varepsilon \left(\frac{5}{8} \frac{M}{r} + \frac{5}{4} \frac{M^2}{r^2} + \frac{5}{2} \frac{M^3}{r^3} + \frac{5M^4}{r^4}\right.\right.$$

$$\left.\left. + \frac{10M^5}{r^5} + \frac{20M^6}{r^6}\right)\right], \tag{C6}$$

where we used $\delta N = -108M^6/r^6$.

APPENDIX D: THE TORTOISE COORDINATE

In this Appendix, we analyze in detail the properties of the tortoise coordinate x, defined in Eq. (16),

$$dx/dr = 1/(Nf).$$

We use the resummation recipe introduced in Sec. II B and detailed in Appendix C to rewrite Eq. (16) as

$$\frac{dx}{dr} = \left(1 - \frac{r_h}{r}\right)^{-1} \left[1 + \varepsilon \left(\frac{5}{8} \frac{M}{r} + \frac{5}{4} \frac{M^2}{r^2} + \frac{5}{52} \frac{M^3}{r^3}\right.\right.$$

$$\left.\left. + \frac{5M^4}{r^4} + \frac{10M^5}{r^5} - \frac{88M^6}{r^6}\right)\right]. \tag{D1}$$

This differential equation can be solved analytically, and the solution can be schematically written as

$$x = r + r_h \log(r/r_h - 1) + \varepsilon \delta x(r), \tag{D2}$$

where we set the integration constant to be $-r_h \log r_h$. The expression for δx is somewhat lengthy and we omit it for brevity. In the limit of general relativity ($\varepsilon = 0$), we recover the usual Schwarzschild formula

$$x = r + 2M \log[r/(2M) - 1]. \tag{D3}$$

For x to be a bona fide tortoise coordinate, we expect that $x \to -\infty$ as $r \to r_h$ and that $x \to \infty$ as $r \to \infty$. Whether this is the case for all values of ε is not immediately evident. Let us first consider the limit of spatial infinity. In this limit, an expansion of Eq. (D2) yields:

$$x \simeq r + r_h \left(1 + \varepsilon \frac{5}{8} \frac{M}{r_h}\right) \log r, \quad \text{for } r/r_h \gg 1. \tag{D4}$$

Because the term in parentheses is $\mathcal{O}(1)$, and because r grows faster than $\log r$, we conclude that $x \to \infty$ when $r \to \infty$, as desired.

We now consider the near-horizon limit. In this limit, an expansion of Eq. (D2) yields:

$$x \simeq r_h + r_h \log(r - r_h) + \varepsilon r_h[p_0 + p_1 \log r_h$$

$$+ p_2 \log(r - r_h)], \quad \text{for } r/r_h \sim 1, \tag{D5}$$

where p_i ($i = 1, 2, 3$) are sextic polynomials in M/r. The coefficients in the polynomials are not all positive, and, consequently, we need to look whether $x \to -\infty$ as $r \to r_h$ in more detail. We first note that the dominant terms in Eq. (D5) for $r \approx r_h$ are those proportional to $\log(r - r_h)$, i.e.,

$$x \simeq r_h(1 + \varepsilon p_2) \log(r - r_h), \tag{D6}$$

where p_2 is:

$$p_2 = \frac{5}{8}\frac{M}{r_{\rm h}} + \frac{5}{4}\frac{M^2}{r_{\rm h}^2} + \frac{5}{2}\frac{M^3}{r_{\rm h}^3} + \frac{5M^4}{r_{\rm h}^4} + \frac{10M^5}{r_{\rm h}^5} - \frac{88M^6}{r_{\rm h}^6}. \quad (D7)$$

In units in which $M = 1$ and for $r_{\rm h} \approx 2$ [cf. Eq. (9)], p_2 has a magnitude of $\mathcal{O}(10^{-1})$. Hence, depending on the value of ε, x can approach either $\pm\infty$ in the limit $r \to r_{\rm h}$. Numerically, we found that $1 + \varepsilon p_2$ becomes negative for $\varepsilon \gtrsim 0.59$. This value of ε is one order of magnitude larger than the values we considered in the main text. Hence, x, as given by Eq. (D2), has the desired properties of a tortoise coordinate for all practical purposes.

APPENDIX E: COEFFICIENTS IN THE EFFECTIVE POTENTIAL

In this Appendix, we present the coefficients $v_{i\ell}^{(\pm)}$ that appear in the EFT corrections $\delta V_\ell^{(\pm)}$ to the Zerilli and Regge-Wheeler potentials (20). The coefficients $v_{i\ell}^{(+)}$ in the polar-parity potential are

$$v_{1\ell}^{(+)} = -5\lambda_\ell^2(\lambda_\ell + 1),$$
$$v_{2\ell}^{(+)} = -5\lambda_\ell^2(2\lambda_\ell + 5),$$
$$v_{3\ell}^{(+)} = -5\lambda_\ell(4\lambda_\ell^2 + 10\lambda_\ell + 9),$$
$$v_{4\ell}^{(+)} = -5(8\lambda_\ell^3 + 20\lambda_\ell^2 + 18\lambda_\ell + 9), \quad (E1)$$

$$v_{5\ell}^{(+)} = 10[-8\lambda_\ell^3 - 20\lambda_\ell^2 - 18\lambda_\ell - 288\lambda_\ell^3(\ell^2 + \ell - 6)/\Lambda_\ell - 9],$$
$$v_{6\ell}^{(+)} = 4\{176\lambda_\ell^3 + 116\lambda_\ell^2 - 90\lambda_\ell$$
$$+ 54\lambda_\ell^2[15\ell^2(\ell+1)^2 - 336\ell(\ell+1) + 836]/\Lambda_\ell - 45\},$$
$$v_{7\ell}^{(+)} = 24\{88\lambda_\ell^2 - 30\lambda_\ell + 15\lambda_\ell[147\ell^2(\ell+1)^2$$
$$- 1304\ell(\ell+1) + 2164]/\Lambda_\ell - 15\},$$
$$v_{8\ell}^{(+)} = 144\{-5 + 44\lambda_\ell + 3\lambda_\ell[1073\ell(\ell+1) - 3988]/\Lambda_\ell\},$$
$$v_{9\ell}^{(+)} = 6336 + [778608\ell(\ell+1) - 1938240]/\Lambda_\ell,$$
$$v_{10\ell}^{(+)} = 879552/\Lambda_\ell.$$

The coefficients $v_{i\ell}^{(-)}$ in the axial-parity potential are

$$v_{1\ell}^{(-)} = -\frac{5}{8}\ell(\ell+1),$$
$$v_{2\ell}^{(-)} = -\frac{5}{4}(\ell^2 + \ell - 3),$$
$$v_{3\ell}^{(-)} = -\frac{5}{2}(\ell^2 + \ell - 3),$$
$$v_{4\ell}^{(-)} = -5(\ell^2 + \ell - 3),$$
$$v_{5\ell}^{(-)} = 1430\ell(\ell+1) - 8610,$$
$$v_{6\ell}^{(-)} = 41460 - 3332\ell(\ell+1),$$
$$v_7^{(-)} = -48192. \quad (E2)$$

We recall that λ_ℓ and Λ_ℓ, appearing in Eqs. (E1) and (E2), are defined in Eq. (19).

[1] T. Regge and J. A. Wheeler, Stability of a Schwarzschild singularity, Phys. Rev. **108**, 1063 (1957).

[2] C. V. Vishveshwara, Stability of the Schwarzschild metric, Phys. Rev. D **1**, 2870 (1970).

[3] M. Davis and R. Ruffini, Gravitational radiation in the presence of a Schwarzschild black hole. A boundary value search, Lett. Nuovo Cimento **2**, 1165 (1971).

[4] M. Davis, R. Ruffini, W. H. Press, and R. H. Price, Gravitational radiation from a particle falling radially into a Schwarzschild black hole, Phys. Rev. Lett. **27**, 1466 (1971).

[5] M. Davis, R. Ruffini, and J. Tiomno, Pulses of gravitational radiation of a particle falling radially into a Schwarzschild black hole, Phys. Rev. D **5**, 2932 (1972).

[6] C. T. Cunningham, R. H. Price, and V. Moncrief, Radiation from collapsing relativistic stars. I—Linearized odd-parity radiation, Astrophys. J. **224**, 643 (1978).

[7] C. T. Cunningham, R. H. Price, and V. Moncrief, Radiation from collapsing relativistic stars. II. Linearized even parity radiation, Astrophys. J. **230**, 870 (1979).

[8] S. Chandrasekhar and S. L. Detweiler, The quasi-normal modes of the Schwarzschild black hole, Proc. R. Soc. A **344**, 441 (1975).

[9] F. J. Zerilli, Effective potential for even-parity Regge-Wheeler gravitational perturbation equations, Phys. Rev. Lett. **24**, 737 (1970).

[10] F. J. Zerilli, Gravitational field of a particle falling in a Schwarzschild geometry analyzed in tensor harmonics, Phys. Rev. D **2**, 2141 (1970).

[11] E. W. Leaver, Spectral decomposition of the perturbation response of the Schwarzschild geometry, Phys. Rev. D **34**, 384 (1986).

[12] Y. Sun and R. H. Price, Excitation of quasinormal ringing of a Schwarzschild black hole, Phys. Rev. D **38**, 1040 (1988).

[13] Y. Sun and R. H. Price, Excitation of Schwarzschild quasinormal modes by collapse, Phys. Rev. D **41**, 2492 (1990).

[14] N. Andersson, Excitation of Schwarzschild black hole quasinormal modes, Phys. Rev. D **51**, 353 (1995).

[15] H.-P. Nollert and R. H. Price, Quantifying excitations of quasinormal mode systems, J. Math. Phys. (N.Y.) **40**, 980 (1999).

[16] K. Glampedakis and N. Andersson, Late time dynamics of rapidly rotating black holes, Phys. Rev. D **64**, 104021 (2001).

[17] E. Berti and V. Cardoso, Quasinormal ringing of Kerr black holes. I. The excitation factors, Phys. Rev. D **74**, 104020 (2006).

[18] Z. Zhang, E. Berti, and V. Cardoso, Quasinormal ringing of Kerr black holes. II. Excitation by particles falling radially with arbitrary energy, Phys. Rev. D **88**, 044018 (2013).

[19] R. H. Price, Nonspherical perturbations of relativistic gravitational collapse. 1. Scalar and gravitational perturbations, Phys. Rev. D **5**, 2419 (1972).

[20] E. W. Leaver, An Analytic representation for the quasi normal modes of Kerr black holes, Proc. R. Soc. A **402**, 285 (1985).

[21] F. Pretorius, Evolution of binary black hole spacetimes, Phys. Rev. Lett. **95**, 121101 (2005).

[22] M. Campanelli, C. O. Lousto, P. Marronetti, and Y. Zlochower, Accurate evolutions of orbiting black-hole binaries without excision, Phys. Rev. Lett. **96**, 111101 (2006).

[23] J. G. Baker, J. Centrella, D.-I. Choi, M. Koppitz, and J. van Meter, Gravitational wave extraction from an inspiraling configuration of merging black holes, Phys. Rev. Lett. **96**, 111102 (2006).

[24] A. Buonanno, G. B. Cook, and F. Pretorius, Inspiral, merger and ring-down of equal-mass black-hole binaries, Phys. Rev. D **75**, 124018 (2007).

[25] S. L. Detweiler, Black holes and gravitational waves. III. The resonant frequencies of rotating holes, Astrophys. J. **239**, 292 (1980).

[26] O. Dreyer, B. J. Kelly, B. Krishnan, L. S. Finn, D. Garrison, and R. Lopez-Aleman, Black hole spectroscopy: Testing general relativity through gravitational wave observations, Classical Quantum Gravity **21**, 787 (2004).

[27] E. Berti, V. Cardoso, and C. M. Will, On gravitational-wave spectroscopy of massive black holes with the space interferometer LISA, Phys. Rev. D **73**, 064030 (2006).

[28] B. P. Abbott *et al.* (LIGO Scientific and Virgo Collaborations), Observation of gravitational waves from a binary black hole merger, Phys. Rev. Lett. **116**, 061102 (2016).

[29] B. P. Abbott *et al.* (LIGO Scientific and Virgo Collaborations), Properties of the binary black hole merger GW150914, Phys. Rev. Lett. **116**, 241102 (2016).

[30] B. P. Abbott *et al.* (LIGO Scientific and Virgo Collaborations), Tests of general relativity with GW150914, Phys. Rev. Lett. **116**, 221101 (2016); **121**, 129902(E) (2018).

[31] S. Endlich, V. Gorbenko, J. Huang, and L. Senatore, An effective formalism for testing extensions to general relativity with gravitational waves, J. High Energy Phys. 09 (2017) 122.

[32] V. Cardoso, M. Kimura, A. Maselli, and L. Senatore, Black holes in an effective field theory extension of general relativity, Phys. Rev. Lett. **121**, 251105 (2018); **131**, 109903(E) (2023).

[33] C. de Rham, J. Francfort, and J. Zhang, Black hole gravitational waves in the effective field theory of gravity, Phys. Rev. D **102**, 024079 (2020).

[34] P. A. Cano, K. Fransen, T. Hertog, and S. Maenaut, Gravitational ringing of rotating black holes in higher-derivative gravity, Phys. Rev. D **105**, 024064 (2022).

[35] P. A. Cano, K. Fransen, T. Hertog, and S. Maenaut, Universal Teukolsky equations and black hole perturbations in higher-derivative gravity, Phys. Rev. D **108**, 024040 (2023).

[36] P. A. Cano, K. Fransen, T. Hertog, and S. Maenaut, Quasinormal modes of rotating black holes in higher-derivative gravity, Phys. Rev. D **108**, 124032 (2023).

[37] K. Glampedakis and N. Andersson, Quick and dirty methods for studying black hole resonances, Classical Quantum Gravity **20**, 3441 (2003).

[38] P. A. Cano and A. Ruipérez, Leading higher-derivative corrections to Kerr geometry, J. High Energy Phys. 05 (2019) 189; 03 (2020) 187.

[39] G. Goon, Heavy fields and gravity, J. High Energy Phys. 01 (2017) 045; 03 (2017) 161(E).

[40] S. Caron-Huot, Y.-Z. Li, J. Parra-Martinez, and D. Simmons-Duffin, Causality constraints on corrections to Einstein gravity, J. High Energy Phys. 05 (2023) 122.

[41] G. T. Horowitz, M. Kolanowski, G. N. Remmen, and J. E. Santos, Extremal Kerr black holes as amplifiers of new physics, Phys. Rev. Lett. **131**, 091402 (2023).

[42] N. Sennett, R. Brito, A. Buonanno, V. Gorbenko, and L. Senatore, Gravitational-wave constraints on an effective field-theory extension of general relativity, Phys. Rev. D **102**, 044056 (2020).

[43] M. Accettulli Huber, A. Brandhuber, S. De Angelis, and G. Travaglini, From amplitudes to gravitational radiation with cubic interactions and tidal effects, Phys. Rev. D **103**, 045015 (2021).

[44] H. O. Silva, A. Ghosh, and A. Buonanno, Black-hole ringdown as a probe of higher-curvature gravity theories, Phys. Rev. D **107**, 044030 (2023).

[45] P. A. Cano, B. Ganchev, D. R. Mayerson, and A. Ruipérez, Black hole multipoles in higher-derivative gravity, J. High Energy Phys. 12 (2022) 120.

[46] R. Cayuso, P. Figueras, T. França, and L. Lehner, Self-consistent modeling of gravitational theories beyond general relativity, Phys. Rev. Lett. **131**, 111403 (2023).

[47] S. Melville, Causality and quasi-normal modes in the GREFT, arXiv:2401.05524.

[48] E. Newman and R. Penrose, An approach to gravitational radiation by a method of spin coefficients, J. Math. Phys. (N.Y.) **3**, 566 (1962).

[49] R. P. Geroch, A. Held, and R. Penrose, A space-time calculus based on pairs of null directions, J. Math. Phys. (N.Y.) **14**, 874 (1973).

[50] A. Hussain and A. Zimmerman, Approach to computing spectral shifts for black holes beyond Kerr, Phys. Rev. D **106**, 104018 (2022).

[51] D. Li, P. Wagle, Y. Chen, and N. Yunes, Perturbations of spinning black holes beyond general relativity: Modified Teukolsky equation, Phys. Rev. X **13**, 021029 (2023).

[52] V. Moncrief, Gravitational perturbations of spherically symmetric systems. I. The exterior problem., Ann. Phys. (N.Y.) **88,** 323 (1974).

[53] S. Chandrasekhar, On one-dimensional potential barriers having equal reflexion and transmission coefficients, Proc. R. Soc. A **369,** 425 (1980).

[54] S. Chandrasekhar, On the potential barriers surrounding the Schwarzschild black-hole, in *Spacetime and Geometry: The Alfred Schild Lectures* (University of Texas Press, Austin, 1982), pp. 120–146.

[55] R. M. Miura, C. S. Gardner, and M. D. Kruskal, Korteweg-de Vries equation and generalizations. II. Existence of conservation laws and constants of motion, J. Math. Phys. (N.Y.) **9,** 1204 (1968).

[56] K. Glampedakis, A. D. Johnson, and D. Kennefick, Darboux transformation in black hole perturbation theory, Phys. Rev. D **96,** 024036 (2017).

[57] M. Lenzi and C. F. Sopuerta, Darboux covariance: A hidden symmetry of perturbed Schwarzschild black holes, Phys. Rev. D **104,** 124068 (2021).

[58] C. de Rham and A. J. Tolley, Causality in curved space-times: The speed of light and gravity, Phys. Rev. D **102,** 084048 (2020).

[59] V. Cardoso, M. Kimura, A. Maselli, E. Berti, C. F. B. Macedo, and R. McManus, Parametrized black hole quasinormal ringdown: Decoupled equations for nonrotating black holes, Phys. Rev. D **99,** 104077 (2019).

[60] N. Andersson, Complex angular momenta and the black hole glory, Classical Quantum Gravity **11,** 3003 (1994).

[61] N. Andersson and K. E. Thylwe, Complex angular momentum approach to black hole scattering, Classical Quantum Gravity **11,** 2991 (1994).

[62] Y. Decanini, A. Folacci, and B. Jensen, Complex angular momentum in black hole physics and the quasinormal modes, Phys. Rev. D **67,** 124017 (2003).

[63] N. Andersson and S. Linnæus, Quasinormal modes of a Schwarzschild black hole: Improved phase-integral treatment, Phys. Rev. D **46,** 4179 (1992).

[64] D. E. Muller, A method for solving algebraic equations using an automatic computer, Math. Tables Aids Comput. **10,** 208 (1956).

[65] K. Ahnert and M. Mulansky, Odeint—solving ordinary differential equations in C++, AIP Conf. Proc. **1389,** 1586 (2011).

[66] Boost C++ Libraries, (https://www.boost.org).

[67] W. H. Press, S. A. Teukolsky, W. T. Vetterling, and B. P. Flannery, *Numerical Recipes 3rd Edition: The Art of Scientific Computing*, 3rd ed. (Cambridge University Press, Cambridge, England, 2007).

[68] P. M. Morse and H. Feshbach, *Methods of Theoretical Physics*, International Series in Pure and Applied Physics (McGraw-Hill, New York, 1953).

[69] N. Andersson, On the asymptotic distribution of quasinormal-mode frequencies for Schwarzschild black holes, Classical Quantum Gravity **10,** L61 (1993).

[70] L. C. Stein, qnm: A Python package for calculating Kerr quasinormal modes, separation constants, and spherical-spheroidal mixing coefficients, J. Open Source Softwaare **4,** 1683 (2019).

[71] G. B. Cook and M. Zalutskiy, Gravitational perturbations of the Kerr geometry: High-accuracy study, Phys. Rev. D **90,** 124021 (2014).

[72] M. Maggiore, The physical interpretation of the spectrum of black hole quasinormal modes, Phys. Rev. Lett. **100,** 141301 (2008).

[73] C. Y. R. Chen, C. de Rham, A. Margalit, and A. J. Tolley, A cautionary case of casual causality, J. High Energy Phys. 03 (2022) 025.

[74] C. Cohen-Tannoudji, B. Diu, and F. Laloë, *Quantum Mechanics* (Wiley-VCH, Wienheim, 1986), Vol. 2.

[75] K. Ioka and H. Nakano, Second and higher-order quasinormal modes in binary black hole mergers, Phys. Rev. D **76,** 061503 (2007).

[76] H. Nakano and K. Ioka, Second order quasi-normal mode of the Schwarzschild black hole, Phys. Rev. D **76,** 084007 (2007).

[77] E. Pazos, D. Brizuela, J. M. Martin-Garcia, and M. Tiglio, Mode coupling of Schwarzschild perturbations: Ringdown frequencies, Phys. Rev. D **82,** 104028 (2010).

[78] L. London, D. Shoemaker, and J. Healy, Modeling ringdown: Beyond the fundamental quasinormal modes, Phys. Rev. D **90,** 124032 (2014); **94,** 069902(E) (2016).

[79] N. Loutrel, J. L. Ripley, E. Giorgi, and F. Pretorius, Second order perturbations of Kerr black holes: Reconstruction of the metric, Phys. Rev. D **103,** 104017 (2021).

[80] J. L. Ripley, N. Loutrel, E. Giorgi, and F. Pretorius, Numerical computation of second order vacuum perturbations of Kerr black holes, Phys. Rev. D **103,** 104018 (2021).

[81] M. H.-Y. Cheung *et al.*, Nonlinear effects in black hole ringdown, Phys. Rev. Lett. **130,** 081401 (2023).

[82] K. Mitman *et al.*, Nonlinearities in black hole ringdowns, Phys. Rev. Lett. **130,** 081402 (2023).

[83] B. Bucciotti, A. Kuntz, F. Serra, and E. Trincherini, Nonlinear quasi-normal modes: Uniform approximation, J. High Energy Phys. 12 (2023) 048.

[84] H.-P. Nollert, Quasinormal modes of Schwarzschild black holes: The determination of quasinormal frequencies with very large imaginary parts, Phys. Rev. D **47,** 5253 (1993).

[85] L. Motl, An analytical computation of asymptotic Schwarzschild quasinormal frequencies, Adv. Theor. Math. Phys. **6,** 1135 (2003).

[86] L. Motl and A. Neitzke, Asymptotic black hole quasinormal frequencies, Adv. Theor. Math. Phys. **7,** 307 (2003).

[87] A. Maassen van den Brink, WKB analysis of the Regge-Wheeler equation down in the frequency plane, J. Math. Phys. (N.Y.) **45,** 327 (2004).

[88] N. Andersson and C. J. Howls, The asymptotic quasinormal mode spectrum of nonrotating black holes, Classical Quantum Gravity **21,** 1623 (2004).

[89] S. Mano, H. Suzuki, and E. Takasugi, Analytic solutions of the Regge-Wheeler equation and the post-Minkowskian expansion, Prog. Theor. Phys. **96,** 549 (1996).

[90] S. Mano, H. Suzuki, and E. Takasugi, Analytic solutions of the Teukolsky equation and their low frequency expansions, Prog. Theor. Phys. **95,** 1079 (1996).

[91] R. Fujita and H. Tagoshi, New numerical methods to evaluate homogeneous solutions of the Teukolsky equation, Prog. Theor. Phys. **112**, 415 (2004).

[92] N. Andersson, Evolving test fields in a black hole geometry, Phys. Rev. D **55**, 468 (1997).

[93] H. O. Silva, G. Tambalo, K. Glampedakis, and K. Yagi, Gravitational radiation from a particle plunging into a Schwarzschild black hole: Frequency-domain and semi-relativistic analyses, Phys. Rev. D **109**, 024036 (2024).

[94] A. Le Tiec and L. Blanchet, The close-limit approximation for black hole binaries with post-Newtonian initial conditions, Classical Quantum Gravity **27**, 045008 (2010).

[95] S. Hirano, M. Kimura, M. Yamaguchi, and J. Zhang, Parametrized black hole quasinormal ringdown formalism for higher overtones, arXiv:2404.09672.

[96] J. L. Jaramillo, R. Panosso Macedo, and L. Al Sheikh, Pseudospectrum and black hole quasinormal mode instability, Phys. Rev. X **11**, 031003 (2021).

[97] J. M. Aguirregabiria and C. V. Vishveshwara, Scattering by black holes: A simulated potential approach, Phys. Lett. A **210**, 251 (1996).

[98] H.-P. Nollert, About the significance of quasinormal modes of black holes, Phys. Rev. D **53**, 4397 (1996).

[99] H. O. Silva, G. Tambalo, K. Glampedakis, K. Yagi, and J. Steinhoff (to be published).

[100] D. Brizuela, J. M. Martin-Garcia, and G. A. Mena Marugan, xPert: Computer algebra for metric perturbation theory, Gen. Relativ. Gravit. **41**, 2415 (2009).

[101] J. M. Martin-Garcia, R. Portugal, and L. R. U. Manssur, The Invar Tensor Package, Comput. Phys. Commun. **177**, 640 (2007).

[102] J. M. Martin-Garcia, D. Yllanes, and R. Portugal, The Invar tensor package: Differential invariants of Riemann, Comput. Phys. Commun. **179**, 586 (2008).

[103] J. M. Martin-Garcia, xPerm: Fast index canonicalization for tensor computer algebra, Comput. Phys. Commun. **179**, 597 (2008).

[104] xAct: Efficient tensor computer algebra for the Wolfram Language, http://www.xact.es/.

[105] Black Hole Perturbation Toolkit (bhptoolkit.org).

[106] H. Stephani, D. Kramer, M. MacCallum, C. Hoenselaers, and E. Herlt, *Exact Solutions of Einstein's Field Equations* (Cambridge University Press, Cambridge, England, 2003).

[107] M. Campanelli, C. O. Lousto, and Y. Zlochower, Algebraic classification of numerical spacetimes and black-hole-binary remnants, Phys. Rev. D **79**, 084012 (2009).